Modeling induced polarization with classical Drude oscillators: Theory and molecular dynamics simulation algorithm

Guillaume Lamoureux
Département de Physique, Université de Montréal, C.P. 6128, succ. Centre-Ville, Montréal, Québec H3C 3J7, Canada

Benoît Roux[a)]
Department of Biochemistry, Weill Medical College of Cornell University, New York, New York 10021

(Received 11 February 2003; accepted 15 May 2003)

A simple treatment for incorporating induced polarization in computer simulations is formulated on the basis of the classical Drude oscillator model. In this model, electronic induction is represented by the displacement of a charge-carrying massless particle attached to a polarizable atom under the influence of the local electric field. The traditional self-consistent field (SCF) regime of induced polarization is reproduced if these auxiliary particles are allowed to relax instantaneously to their local energy minima for any given fixed configuration of the atoms in the system. In practice, such treatment is computationally prohibitive for generating molecular dynamics trajectories because the electric field must be recalculated several times iteratively to satisfy the SCF condition, and it is important to seek a more efficient way to simulate the classical Drude oscillator model. It is demonstrated that a close approximation to the SCF regime can be simulated efficiently by considering the dynamics of an extended Lagrangian in which a small mass is attributed to the auxiliary particles, and the amplitude of their oscillations away from the local energy minimum is controlled with a low-temperature thermostat. A simulation algorithm in this modified two-temperature isobaric–isothermal ensemble is developed. The algorithm is tested and illustrated using a rigid three-site water model with one additional Drude particle attached to the oxygen which is closely related to the polarizable SPC model of Ahlström *et al.* [Mol. Phys. **68**, 563 (1989)]. The tests with the extended Lagrangian show that stable and accurate molecular dynamics trajectories for large integration time steps (1 or 2 fs) can be generated and that liquid properties equivalent to SCF molecular dynamics can be reproduced at a fraction of the computational cost. © *2003 American Institute of Physics.* [DOI: 10.1063/1.1589749]

I. INTRODUCTION

Most computer simulations of biomolecular systems are generated using simple potential functions which do not account for many-body induced polarization effects explicitly. Induced polarization, which arises from a perturbation of the electronic structure of the molecular species in response to external electric fields, is typically incorporated in these simulations in an average effective way. For example, widely used potential functions such as AMBER/parm94,[1] CHARMM27,[2] GROMOS,[3] and OPLS[4] force fields are based on pairwise additive electrostatic interactions with fixed effective atomic partial charges. Typically, the magnitude of the atomic partial charges has been adjusted to account for the average induction arising in a typical environment. Despite the apparent simplification, such potential functions have been remarkably successful in modeling complex molecular systems over the last two decades (e.g., see Ref. 5 and references therein). For example, the properties of liquid water can be represented quite realistically without introducing induced polarizability explicitly if the dipole moment of the water molecule is enhanced compared to its gas phase value of 1.85 D, e.g., 2.35 D for TIP3P,[6] 2.27 D for SPC,[7] 2.18 D for TIP4P,[6] and 2.29 D for TIP5P.[8] Furthermore, such effective nonpolarizable potential functions are also able to reproduce the solvation free energy of small cations quite well,[9,10] although there are some difficulties with anions.[11–14] Nonetheless, these potential functions are clearly limited in their ability to model complex biological systems such as membrane ion channels,[15] and despite their usefulness there are growing concerns about their shortcomings in general.[16]

In recent years, there have been increasing efforts dedicated to develop models that account for induced polarization more accurately. Most of the current models for incorporating polarizability into a potential function belong to one of three classes:[16,17] point dipole induction models, charge transfer models (or fluctuating charge models), and classical Drude oscillator models (or shell models). The main drawback of any treatment of induced polarization comes from the computationally expensive convergence of the self-consistent field (SCF) condition, which must be satisfied at each molecular dynamics time step to determine the magnitude of the induction and the atomic forces. The SCF condition follows directly from the Born–Oppenheimer approximation, which assumes that the (quantum) electronic degrees

a)Electronic mail: benoit.roux@med.cornell.edu

of freedom must relax instantaneously to their ground state for every configuration of the nuclei. It is possible, however, to avoid the iterative SCF procedure altogether and to reduce the computational cost of induced polarization by treating the induction ''variables'' as part of the (classical) dynamical variables in an extended Lagrangian representation.[18,19] Although such computational schemes are efficient and very attractive, the significance of the results obtained from simulations in which the induction variables are allowed to undergo unphysical classical thermal fluctuations is not completely clear.

The traditional point dipole induction model for liquids has a long history which goes back to Kirkwood and Onsager,[20,21] and it is, arguably, one of the most natural way to incorporate polarizability in molecular mechanical force fields (e.g., see Refs. 11, 18, 22–25). In this representation, atoms are assigned fixed atomic charges and inducible dipoles, which are then self-consistently adjusted for any given configuration of the atoms in the systems. Such a simple model can correctly capture the polarizability in a variety of systems, e.g., organic molecules,[26–28] amino acids,[29] and ions in water.[25] The main drawback of this approach are the inconveniences arising from the (cumbersome) vectorial character of the point dipole and the significant modifications of the molecular mechanical force field that it requires in standard biomolecular simulation programs. Notably, the constant-pressure algorithm and the fast particle-mesh-Ewald (PME) summation procedure[30,31] have to be extended and generalized to include charge–dipole and dipole–dipole interactions. Despite these technical difficulties, an initial version of an atomic point dipole model has been recently implemented for the AMBER/parm02 polarizable force field.[32]

Charge transfer models treat the atomic partial charges as quantities allowed to vary according to a self-consistent atomic electronegativity equalization scheme.[33–35] Such models are attractive compared to point dipole induction models because they require no particular overhead in the computation of the atomic forces, since simple charge–charge Coulomb laws are maintained. Charge transfer models can, however, be seriously limited in their ability to represent the different components of the polarizability tensor of some molecular species accurately. For example, a linear molecule can only be polarized along its axis, and a planar molecule has a zero transverse polarizability. Charge transfer models were shown to be successful for liquid water,[19] but unable to represent a bifurcated hydrogen bond or the transverse polarization of an aromatic ring without the addition of inducible dipoles.[28] As pointed out by Chelli *et al.*,[36] atom-based charge transfer models may also considerably overestimate the polarizability of biopolymers by allowing charge to flow between remote atoms at too small an energy cost. For large molecules, it is necessary to impose further constraints to limit charge transfer to neighboring atoms.[28,36,37]

The Drude oscillator model, which was originally proposed by Paul Drude in 1900 as a simple way to describe the dispersive properties of materials,[38] represents electronic induction by introducing a massless charged particle, attached to each polarizable atom by a harmonic spring. The position of these ''auxiliary'' particles is then adjusted self-consistently to their local energy minima for any given configuration of the atoms in the system. A quantum version of the model has been used in early applications to describe the dipole–dipole dispersion interactions.[39–41] A semiclassical version of the model was used more recently to describe molecular interactions,[42] and electron binding.[43] The classical version of the model has been quite useful in statistical mechanical studies of dense systems, e.g., ionic crystals,[44–49] simple liquids of polarizable particles,[50–53] liquid water,[54–58] and the hydration of small ions.[12,59] One particularly attractive aspect of the Drude oscillator model is that it preserves the simple charge–charge Coulomb electrostatic interaction. Its implementation in standard biomolecular simulation programs is, therefore, relatively straightforward (including constant-pressure algorithm and PME electrostatics). Despite this technical advantage, Drude oscillators have not been as widely used as the point dipole or charge transfer models, probably because of the difficulties designing efficient computational schemes to solve the fast motion of the auxiliary particles in molecular dynamics simulations.[58] One may note that, in contrast with the point dipole[18] and charge transfer models,[19,60] extended dynamics algorithms have not been implemented to simulate Drude oscillator models, and that applications to liquids have usually relied on a direct SCF iterative scheme.

In this paper, we formulate a simple polarizable model based on Drude oscillators and explore its theoretical features. In particular, the consequences of allowing the Drude particles to undergo classical thermal fluctuations is clarified. Furthermore, we present an efficient numerical integration procedure based on an extended Lagrangian technique for generating accurate molecular dynamics trajectories. The accuracy and efficiency of the simulation algorithm is illustrated by using a Drude oscillator version of the polarizable SPC (PSPC) model of Ahlström *et al.*[61] It is shown that the trajectories generated by the extended dynamics algorithm are nearly equivalent to those generated using a rigorous SCF procedure. The paper is concluded with a summary of the main points and an overview of future work.

II. MOLECULAR DYNAMICS OF THE POLARIZABLE ATOMS

A. Drude oscillator model

To model the polarizability α of a given atom with partial charge q, a mobile Drude particle carrying a charge q_D is introduced. The charge of the atom is replaced by $q-q_D$ to preserve the net charge of the atom–Drude pair. The Drude particle is harmonically bound to the atomic particle with a force constant k_D, which is assumed to be the same for all atoms without any loss of generality. In the absence of a field, the Drude particle oscillates around the position of the atom, $\mathbf{r}$, and the atom appears on average as a point charge q. In a uniform field $\mathbf{E}$, the Drude particle oscillates around a displaced position $\mathbf{r}+\mathbf{d}$ with $\mathbf{d}=q_D\mathbf{E}/k_D$, and the average induced atomic dipole is $\boldsymbol{\mu}=q_D^2\mathbf{E}/k_D$. It follows that the isotropic atomic polarizability has a simple expression

$$\alpha = \frac{q_D^2}{k_D}. \tag{1}$$

For a given α, the force constant k_D can be chosen such that the displacement $\mathbf{d}$ of the Drude particle remains much smaller than any interatomic distance, and that the resulting induced dipole $\boldsymbol{\mu}$ is almost equivalent to a point dipole. Within this point–dipole approximation, the only relevant parameter is the combination q_D^2/k_D.

More generally, adding auxiliary Drude particles to a system of atoms yields the polarizable force field

$$U(\{\mathbf{r}\},\{\mathbf{d}\}) = U_{\text{self}}(\{\mathbf{d}\}) + U_{\text{bond}}(\{\mathbf{r}\}) + U_{\text{elec}}(\{\mathbf{r}\},\{\mathbf{d}\}) + U_{\text{LJ}}(\{\mathbf{r}\}), \tag{2}$$

where $U_{\text{self}}(\{\mathbf{d}\})$ represents the atom–Drude harmonic bonds (the $\frac{1}{2}kd^2$ terms), $U_{\text{bond}}(\{\mathbf{r}\})$ is the intramolecular energy contribution from the bond lengths, angles, and dihedrals, $U_{\text{elec}}(\{\mathbf{r}\},\{\mathbf{d}\})$ represents all Coulombic interactions (atom–atom, atom–Drude, and Drude–Drude), and $U_{\text{LJ}}(\{\mathbf{r}\})$ is a Lennard-Jones "12–6" nonpolar contribution.

B. Self-consistent field regime

To implement the self-consistent field (SCF) condition corresponding to the Born–Oppenheimer approximation, the forces acting on the nuclei must be computed after the Drude particles have relaxed to minimize the total potential energy. For a given nuclear configuration of N polarizable atoms, $\{\mathbf{r}\}$, the relaxed Drude particle positions $\{\mathbf{r}+\mathbf{d}^{\text{SCF}}\}$ are found by solving

$$\frac{\partial U}{\partial \mathbf{d}_i} = \mathbf{0}, \tag{3}$$

where U is the force field of Eq. (2) and where index i runs from 1 to N. U_{bond} and U_{LJ} are independent of the $\mathbf{d}$'s, and

$$\frac{\partial U_{\text{self}}}{\partial \mathbf{d}_i} + \frac{\partial U_{\text{elec}}}{\partial \mathbf{d}_i} = \mathbf{0}. \tag{4}$$

These equations define the force equilibria on the Drude particles

$$k_D\mathbf{d}_i - q_{D,i}\mathbf{E}_i = \mathbf{0}, \tag{5}$$

where $\mathbf{E}_i$ is the total electric field in $\mathbf{r}_i+\mathbf{d}_i$, arising from the fixed charges as well as all the induced dipoles (modeled with Drude oscillators). In the point–dipole approximation, these conditions can be rewritten as the familiar self-consistent equations for induced polarization[62]

$$\boldsymbol{\mu}_i^{\text{SCF}} = \alpha_i\left[-\sum_{j\neq i} q_j \boldsymbol{\nabla}_i\left(\frac{1}{r_{ij}}\right) + \sum_{j\neq i} \boldsymbol{\mu}_j^{\text{SCF}}\cdot\boldsymbol{\nabla}_i\boldsymbol{\nabla}_i\left(\frac{1}{r_{ij}}\right)\right]. \tag{6}$$

(See Appendix A for details.) For atomic positions $\{\mathbf{r}\}$, the relaxed displacements produce the potential

$$U^{\text{SCF}}(\{\mathbf{r}\}) \equiv U(\{\mathbf{r}\},\{\mathbf{d}^{\text{SCF}}\}), \tag{7}$$

and the atomic motions in the SCF regime are described by

$$m_i\ddot{\mathbf{r}}_i = -\frac{\partial U^{\text{SCF}}}{\partial \mathbf{r}_i}. \tag{8}$$

Integrating Eq. (8) with molecular dynamics requires that the positions of the Drude particles be set at their energy minimum at every integration time step, by solving Eq. (5). This simple simulation method has been widely used in molecular dynamics[47,49,57,63] as well as in Monte Carlo simulations.[54,56,64] Nonetheless, the SCF procedure is limited and computationally expensive, because any nonconverged energy minimization introduces systematic drag forces on the physical atoms that considerably affect energy conservation and the stability of the temperature.[47,49,58]

C. Thermalized Drude oscillators

A simple alternative to SCF is to extend the Lagrangian of the system to consider dipoles as additional dynamical degrees of freedom. This extended dynamics approach was proposed by Sprik and Klein[60] for inducible dipoles described as fluctuating charges placed on a small tetrahedron following rigidly each water molecule. A similar extended system was proposed by van Belle *et al.* for inducible point dipoles.[65,66] In the present system, the additional degrees of freedom are the positions of the moving Drude particles. All Drude particles are attributed a small mass m_D, taken from the atomic masses $\{m_i\}$, and the motion of atoms and Drude particles (at positions $\{\mathbf{r}_i\}$ and $\{\mathbf{r}_{D,i}\equiv\mathbf{r}_i+\mathbf{d}_i\}$) is simulated on an equal dynamical footing

$$(m_i - m_D)\ddot{\mathbf{r}}_i = -\frac{\partial U}{\partial \mathbf{r}_i}, \tag{9}$$

$$m_D\ddot{\mathbf{r}}_{D,i} = -\frac{\partial U}{\partial \mathbf{r}_{D,i}}. \tag{10}$$

The motion of Drude particles is expected to be decoupled from the atomic motion if m_D is sufficiently small. The obvious drawback is that a small m_D requires a small integration time step.[48,55,67] For a single Drude oscillator, a significant speedup recovery can be attained by using a multi-time-step integration approach,[12,59] but this advantage is lost for a dense system of polarizable atoms, because the long-range $1/r^3$ dipole–dipole interactions include high-frequency oscillations and have to be integrated using the shortest time step. Provided a relaxed initial configuration obeying Eq. (5), the Drude oscillators will follow a quasiadiabatic dynamics. However, even if m_D is very small, the Drude particles will eventually reach a thermal equilibrium with the rest of the system. Therefore, simulation approaches relying solely on the kinetic decoupling of the Drude oscillators to maintain a Born–Oppenheimer regime are inappropriate for long simulation runs. Taking advantage of the long thermalization time, it is possible to remain close to the SCF energy surface by periodically resetting the positions of the Drude oscillators to their energy minimum.[12] But, doing so makes the simulation irreversible.

From this point of view, it is of interest to examine the consequences of full thermalization of the classical Drude oscillators on the properties of the system. This is particularly important given the fact that any classical fluctuations of the Drude oscillators are *a priori* unphysical according to the Born–Oppenheimer approximation, upon which electronic induction models are based. One way to address this

question is to determine the statistical probability of the nuclear configuration $\{\mathbf{r}\}$ under the influence of thermally fluctuating Drude oscillators. Because such system is concerned only with classical degrees of freedom (nuclei and Drude oscillators), this task is trivial. The probability of any nuclear configuration is proportional to the Boltzmann factor of an effective potential of mean force, $e^{-\beta U^{\mathrm{eff}}}$, which is rigorously obtained by integrating out the displacements of the Drude oscillators

$$e^{-\beta U^{\mathrm{eff}}(\{\mathbf{r}\})} = \frac{\int d\{\mathbf{d}\}\, e^{-\beta U(\{\mathbf{r}\},\{\mathbf{d}\})}}{\int d\{\mathbf{d}\}\, e^{-\beta U_{\mathrm{self}}(\{\mathbf{d}\})}}. \tag{11}$$

Decomposing the displacements $\{\mathbf{d}\}$ in terms of the SCF displacements $\{\mathbf{d}^{\mathrm{SCF}}\}$ and the thermal fluctuations $\{\delta\mathbf{d}\}$, the potential energy U can be expanded in powers of $\{\delta\mathbf{d}\}$

$$U(\{\mathbf{r}\},\{\mathbf{d}\}) = U^{\mathrm{SCF}}(\{\mathbf{r}\}) + \sum_i \delta\mathbf{d}_i \cdot \left.\frac{\partial U}{\partial \mathbf{d}_i}\right|_{\mathrm{SCF}} + \frac{1}{2}\sum_{ij} \delta\mathbf{d}_i \cdot \left.\frac{\partial^2 U}{\partial \mathbf{d}_i \partial \mathbf{d}_j}\right|_{\mathrm{SCF}} \cdot \delta\mathbf{d}_j + \cdots. \tag{12}$$

In the point–dipole approximation, only the first- and second-order terms are nonzero. The SCF contribution to the interaction can be factored out, and the first-order terms average to zero

$$e^{-\beta U^{\mathrm{eff}}(\{\mathbf{r}\})} = e^{-\beta U^{\mathrm{SCF}}(\{\mathbf{r}\})} \times \frac{\int d\{\delta\mathbf{d}\}\, e^{-(1/2)\beta \Sigma_{ij} \delta\mathbf{d}_i \cdot (\partial^2 U/\partial \mathbf{d}_i \partial \mathbf{d}_j)\cdot \delta\mathbf{d}_j}}{\int d\{\delta\mathbf{d}\}\, e^{-\beta U_{\mathrm{self}}(\{\delta\mathbf{d}\})}}. \tag{13}$$

The remaining integral can be evaluated as a moment expansion. Truncating the expansion to two-body interactions yields

$$U^{\mathrm{eff}}(\{\mathbf{r}\}) = U^{\mathrm{SCF}}(\{\mathbf{r}\}) - \frac{3}{2} k_{\mathrm{B}} T \sum_{ij} \frac{\alpha_i \alpha_j}{r_{ij}^6} + \cdots. \tag{14}$$

(See Appendix B for the details of the calculation.) In addition to the static induction effects included in U^{SCF}, the thermalized (''hot'') Drude oscillators give rise to a $1/r^6$, temperature-dependent, attractive term. This $\frac{3}{2}k_{\mathrm{B}}T\alpha^2/r^6$ term is the classical thermodynamic equivalent of the London quantum dispersive attraction $E_{\mathrm{I}}\alpha^2/r^6$.[39] It corresponds to a small perturbation to the London forces, because $k_{\mathrm{B}}T$ is at least two orders of magnitude smaller than the typical ionization energy E_{I}. The smaller the temperature of the dipole motion is, the closer the effective potential is to the SCF potential. Equation (14) is independent of m_{D}, the mass of the oscillators. This is an indication that the argument it makes concerning a system of thermalized Drude oscillators applies to the thermodynamic properties but not to the dynamic properties.

D. Low-temperature Drude oscillators

To approximately reproduce the dynamics equivalent to the SCF regime of Eq. (8), we use two Nosé–Hoover thermostats:[68] a first one to keep the atoms at room temperature T and a second one to reduce the thermal fluctuations of the Drude oscillators by imposing a temperature $T_\star \ll T$. The idea of cooling the polarization degrees of freedom with a separate thermostat was carefully studied by Sprik,[69] who showed that, for cold dipoles, both the equilibrium and diffusion properties are independent of the value of the dipole inertia parameter (the analog of m_{D}), as long as it is sufficiently small. For Drude oscillators, the temperature $T_\star$ should be small enough to leave almost no kinetic energy to the atom–Drude vibrations, yet large enough to allow the Drude particles to readjust to the room-temperature motion of the atoms.

The second thermostat is coupled to the motion of the Drude particles relative to their nuclei, $\{\dot{\mathbf{d}}\}$ (not to their absolute motion $\{\dot{\mathbf{r}}_{\mathrm{D}}\}$). Denoting $\mathbf{R}_i$ the center of mass of each $(\mathbf{r}_i, \mathbf{r}_{\mathrm{D},i})$ pair, m_i the total mass of the pair (as before), and $m_i' = m_{\mathrm{D}}(1 - m_{\mathrm{D}}/m_i)$ the reduced mass, the equations of motion are

$$m_i \ddot{\mathbf{R}}_i = \mathbf{F}_{\mathbf{R},i} - m_i \dot{\mathbf{R}}_i \dot{\eta}, \tag{15}$$

$$m_i' \ddot{\mathbf{d}}_i = \mathbf{F}_{\mathbf{d},i} - m_i' \dot{\mathbf{d}}_i \dot{\eta}_\star, \tag{16}$$

$$Q \ddot{\eta} = \sum_j m_j \dot{R}_j^2 - N_{\mathrm{f}} k_{\mathrm{B}} T, \tag{17}$$

$$Q_\star \ddot{\eta}_\star = \sum_j m_j' \dot{d}_j^2 - N_{\mathrm{f}\star} k_{\mathrm{B}} T_\star. \tag{18}$$

Indices i and j run from 1 to N, the total number of atoms. Because not all atoms have to be polarizable, the total number of Drude particles, N_{D}, may be less than N. If a given atom i bears no Drude oscillator, $\mathbf{R}_i$ corresponds to $\mathbf{r}_i$, m_i' is zero, and the corresponding Eq. (16) is ignored. N_{f} is the number of degrees of freedom associated with the atomic motion, accounting for distance constraints imposed by SHAKE,[70] and $N_{\mathrm{f}\star} \equiv 3N_{\mathrm{D}}$ is the number of degrees of freedom associated with the motion of the Drude oscillators. Q and $Q_\star$ are the inertia factors of the Nosé–Hoover thermostats. They are related to characteristic time scales of the motion, τ and $\tau_\star$, via $Q \equiv N_{\mathrm{f}} k_{\mathrm{B}} T \tau^2$ and $Q_\star \equiv N_{\mathrm{f}\star} k_{\mathrm{B}} T_\star \tau_\star^2$. The ''velocities'' $\dot{\eta}$ and $\dot{\eta}_\star$ are acting as friction coefficients, that is, as scaling exponents on the velocities $\{\dot{\mathbf{R}}\}$ and $\{\dot{\mathbf{d}}\}$. They are driven by ''forces'' G and $G_\star$—the right-hand sides of Eqs. (17) and (18), respectively—opposing any deviation from the target temperatures T and $T_\star$. $\mathbf{F}_{\mathbf{R},i} = -\partial U/\partial \mathbf{R}_i$ and $\mathbf{F}_{\mathbf{d},i} = -\partial U/\partial \mathbf{d}_i$ are the forces on the centers of mass and on the displacements. Using the chain rule, they can be written in terms of the actual forces on the particles

$$\mathbf{F}_{\mathbf{R},i} = -\frac{\partial U}{\partial \mathbf{r}_i} - \frac{\partial U}{\partial \mathbf{r}_{\mathrm{D},i}}, \tag{19}$$

$$\mathbf{F}_{\mathbf{d},i} = -\left(1 - \frac{m_{\mathrm{D}}}{m_i}\right)\frac{\partial U}{\partial \mathbf{r}_{\mathrm{D},i}} + \left(\frac{m_{\mathrm{D}}}{m_i}\right)\frac{\partial U}{\partial \mathbf{r}_i}. \tag{20}$$

The equations of motion (15) and (16) can be formulated in terms of the real coordinates of the particles, using the inverse transformation

$$\mathbf{r}_i = \mathbf{R}_i - \left(\frac{m_\mathrm{D}}{m_i}\right)\mathbf{d}_i, \tag{21}$$

$$\mathbf{r}_{\mathrm{D},i} = \mathbf{R}_i + \left(1 - \frac{m_\mathrm{D}}{m_i}\right)\mathbf{d}_i. \tag{22}$$

The system (15) to (18) conserves the extended energy

$$E_\mathrm{NH} = E + \tfrac{1}{2}Q\dot{\eta}^2 + \tfrac{1}{2}Q_\star\dot{\eta}_\star^2 + N_\mathrm{f}k_\mathrm{B}T\eta + N_{\mathrm{f}\star}k_\mathrm{B}T_\star\eta_\star, \tag{23}$$

where E is the sum of kinetic and potential energies of the particles. The variables η and $\eta_\star$ correspond to specific energies in each of the heat baths, from an arbitrary reference level. Steady heat flows are expected from the Drude oscillators to the cold bath $T_\star$ and from the room-temperature bath T to the atoms, that is, $\langle\dot{\eta}_\star\rangle > 0$ and $\langle\dot{\eta}\rangle < 0$. This heat transfer is small if the Drude particles and the atoms have weakly coupled kinetics (e.g., if the power spectra of their velocity autocorrelation functions do not significantly overlap).

Designing an efficient scheme to integrate Eqs. (15) to (18) requires some care. The procedure should conserve energy and simulate the appropriate thermodynamic ensemble as accurately as possible, despite the fact that heat is steadily flowing from the subsystem at room temperature T to the subsystem at $T_\star$. Following Martyna *et al.*,[71] the complete evolution operator over a time step Δt, formally expressed in terms of the total Liouville operator as $e^{i\mathcal{L}\Delta t}$, is decomposed in terms of a "velocity-Verlet" propagation, denoted $e^{i\mathcal{L}_\mathrm{vV}\Delta t}$, and a multistep "Nosé–Hoover" propagation, each step denoted $e^{i\mathcal{L}_\mathrm{NH}\Delta t/2n_\mathrm{c}}$

$$e^{i\mathcal{L}\Delta t} \simeq (e^{i\mathcal{L}_\mathrm{NH}\Delta t/2n_\mathrm{c}})^{n_\mathrm{c}} e^{i\mathcal{L}_\mathrm{vV}\Delta t} (e^{i\mathcal{L}_\mathrm{NH}\Delta t/2n_\mathrm{c}})^{n_\mathrm{c}}. \tag{24}$$

This integration procedure is explained in detail in Ref. 71. The modified version developed for the current model is presented in Appendix C 1.

Because the atomic forces $\{\mathbf{F}\}$ are involved only in the "velocity-Verlet" propagation, each step of the "Nosé–Hoover" propagation is an $O(N)$ calculation and thus n_c can be large without significantly affecting the efficiency. Test simulations show that, for any useful time step Δt and Drude mass m_D (e.g., in the range $\Delta t = 1.0$ fs and $m_\mathrm{D} = 0.5$ amu), the "one-step" ($n_\mathrm{c} = 1$) integrator is not sufficiently accurate. Due to systematic integration errors on the variables $\dot{\eta}$ and $\dot{\eta}_\star$, the temperatures are poorly controlled. Moreover, these errors are accumulating in η and $\eta_\star$, and the extended energy of Eq. (23) is drifting. With $n_\mathrm{c} > 1$, the systematic errors on $\dot{\eta}$ and $\dot{\eta}_\star$ are reduced, and the accuracy of the algorithm is significantly improved at a small computational cost.

E. Constant-pressure dynamics

The modified Andersen–Hoover barostat of Martyna *et al.*[72] was implemented to allow fluctuations in the volume of the system. The system of Eqs. (15) to (18) is further extended to include the barostat variable ε, regulating the internal pressure of the system through isotropic scaling of the simulation cell. Because of this scaling, the evolution of the positions $\{\mathbf{R}, \mathbf{d}\}$ is not directly related to the conjugate velocities $\{\mathbf{v_R}, \mathbf{v_d}\}$. The equations of motion are

$$\dot{\mathbf{R}}_i = \mathbf{v}_{\mathbf{R},i} + \mathbf{R}_i\dot{\varepsilon}, \tag{25}$$

$$m_i\dot{\mathbf{v}}_{\mathbf{R},i} = \mathbf{F}_{\mathbf{R},i} - m_i\mathbf{v}_{\mathbf{R},i}(\dot{\eta} + a\dot{\varepsilon}), \tag{26}$$

$$\dot{\mathbf{d}}_i = \mathbf{v}_{\mathbf{d},i} + \mathbf{d}_i\dot{\varepsilon}, \tag{27}$$

$$m_i'\dot{\mathbf{v}}_{\mathbf{d},i} = \mathbf{F}_{\mathbf{d},i} - m_i'\mathbf{v}_{\mathbf{d},i}(\dot{\eta}_\star + a\dot{\varepsilon}), \tag{28}$$

$$Q\ddot{\eta} = \sum_j m_j v_{\mathbf{R},j}^2 - N_\mathrm{f}k_\mathrm{B}T, \tag{29}$$

$$Q_\star\ddot{\eta}_\star = \sum_j m_j' v_{\mathbf{d},j}^2 - N_{\mathrm{f}\star}k_\mathrm{B}T_\star, \tag{30}$$

$$W\ddot{\varepsilon} = a\sum_j (m_j v_{\mathbf{R},j}^2 + m_j' v_{\mathbf{d},j}^2) + \sum_j (\mathbf{R}_j\cdot\mathbf{F}_{\mathbf{R},j} + \mathbf{d}_j\cdot\mathbf{F}_{\mathbf{d},j}) - 3PV. \tag{31}$$

Implicit in Eq. (25) is the relationship between ε and V, the volume of the simulation cell

$$\dot{V} = 3V\dot{\varepsilon}. \tag{32}$$

For simplicity, the N_D variables $\{\mathbf{d}\}$ are scaled along with the N atomic positions, even though they represent dipoles having almost no thermal fluctuations. Not doing so would require the virial contribution to the pressure, $\mathbf{R}\cdot\mathbf{F_R} + \mathbf{d}\cdot\mathbf{F_d}$, to be replaced by $\mathbf{R}\cdot(\mathbf{F_R} + \mathbf{F_d})$. The right-hand side of Eq. (31) is the driving force of the barostat, correcting for any deviation from the target pressure P. W is the inertia factor of the barostat, related to a time scale τ_ε via $W \equiv N_{\mathrm{f}\varepsilon}k_\mathrm{B}T\tau_\varepsilon^2$. $N_{\mathrm{f}\varepsilon}$ is the number of degrees of freedom effectively contributing to the pressure, that is, $N_\mathrm{f} + N_{\mathrm{f}\star}$ if $T_\star$ equals T, but only N_f if $T_\star$ is much lower than T. Because the center of mass of the whole system is unaffected by the position scaling, three of the $N_{\mathrm{f}\varepsilon}$ degrees of freedom that are explicitly scaled are independent of the volume, and the kinetic contribution to the internal pressure is corrected by a coefficient $a = 1 + 3/N_{\mathrm{f}\varepsilon}$.

The equations of motion (25) to (31) conserve the extended energy

$$E_\mathrm{AH} = E_\mathrm{NH} + \tfrac{1}{2}W\dot{\varepsilon}^2 + PV, \tag{33}$$

where E_NH is defined in Eq. (23). They can be integrated using an extension of the method described in the previous section.[73] The details are given in Appendix C 2.

F. Avoiding the "flying ice cube" problem

Even though the trajectory generated by integrating Eqs. (25) to (31) rigorously conserves the total momentum, a spurious translation of the center of mass of the system may arise after some time due to an accumulation of small numerical error, giving rise to the "flying ice cube" artifact.[74] All water molecules are gradually losing most of their relative thermal motion to develop a large coherent translation. This peculiar phenomenon is consistent with Eqs. (25) to (31), because thermostats are insensitive to how kinetic energy is partitioned among the degrees of freedom. When it is not explicitly enforced by "massive thermostatting,"[75–77] energy equipartition in molecular dynamics comes from the

physical coupling between the different modes of motion. Typically, an excess of kinetic energy in one mode is rapidly distributed among the other modes as a result of the tight coupling. But, an excess of kinetic energy in an uncoupled mode, such as a global translation in periodic boundary conditions, is not redistributed. This could also occur for a global rotation, if the boundary conditions have circular symmetry. In principle, a system with zero total momentum should remain so, since all internal forces have an equal and opposite reaction and no external forces are applied. However, a coherent translation may appear if action and reaction forces show small systematic numerical errors,[78] or if temperature is kept constant by velocity rescaling.[74,78] Numerical imprecision in calculating the long-range electrostatic interactions using PME may also contribute to damaging the conservation of the total momentum.

In the present case, with two competing thermostats, the origin of the flying ice cube artifact is clear. From Eqs. (26) and (28), the center-of-mass motion is

$$M_{\mathrm{tot}}\dot{\mathbf{V}}_{\mathrm{cm}} = -M_{\mathrm{tot}}\mathbf{V}_{\mathrm{cm}}(\dot{\eta}+a\dot{\varepsilon}), \tag{34}$$

where M_{tot} is the total mass of the system. Because $\langle\dot{\eta}\rangle<0$ and $\langle\dot{\varepsilon}\rangle=0$, any nonzero velocity will be systematically amplified, yielding a significant numerical instability. Considering a random force created by numerical errors, $\mathbf{F}_{\mathrm{err}}$, and writing $\dot{\eta}=\langle\dot{\eta}\rangle+\delta\dot{\eta}$, the actual equation of motion of the center of mass is

$$M_{\mathrm{tot}}\dot{\mathbf{V}}_{\mathrm{cm}} \approx \mathbf{F}_{\mathrm{err}} - M_{\mathrm{tot}}\mathbf{V}_{\mathrm{cm}}(\langle\dot{\eta}\rangle+\delta\dot{\eta}+a\dot{\varepsilon}). \tag{35}$$

Assuming that $\mathbf{F}_{\mathrm{err}}$ and $\delta\dot{\eta}+a\dot{\varepsilon}$ are uncorrelated random variables, $\mathbf{V}_{\mathrm{cm}}$ has an unstable behavior around $\mathbf{V}_{\mathrm{cm}}=\mathbf{0}$ as long as $\langle\dot{\eta}\rangle$ is negative, that is, as long as the flying ice cube steady regime is not attained. Even if the center of mass is initially immobile, the numerical errors on the forces will create velocity fluctuations that will be slowly amplified by an exponential factor $e^{|\langle\dot{\eta}\rangle|t}$. To explicitly avoid this problem, the velocities $\{\mathbf{v}_{\mathbf{R}}\}$ in Eqs. (26) and (29) are replaced by $\{\mathbf{v}'_{\mathbf{R}}\}$, relative to the center-of-mass velocity $\mathbf{V}_{\mathrm{cm}}$, and the center-of-mass motion is coupled to a heat sink. Velocities $\{\mathbf{v}_{\mathbf{d}}\}$ are unchanged, because they already are relative to $\mathbf{V}_{\mathrm{cm}}$. The modified system is

$$\dot{\mathbf{R}}_i = \mathbf{v}_{\mathbf{R},i} + \mathbf{R}_i\dot{\varepsilon}, \tag{36}$$

$$m_i\dot{\mathbf{v}}'_{\mathbf{R},i} = \mathbf{F}_{\mathbf{R},i} - m_i\mathbf{v}'_{\mathbf{R},i}(\dot{\eta}+a\dot{\varepsilon}), \tag{37}$$

$$\dot{\mathbf{d}}_i = \mathbf{v}_{\mathbf{d},i} + \mathbf{d}_i\dot{\varepsilon}, \tag{38}$$

$$m'_i\dot{\mathbf{v}}_{\mathbf{d},i} = \mathbf{F}_{\mathbf{d},i} - m'_i\mathbf{v}_{\mathbf{d},i}(\dot{\eta}_\star+a\dot{\varepsilon}), \tag{39}$$

$$M_{\mathrm{tot}}\dot{\mathbf{V}}_{\mathrm{cm}} = -M_{\mathrm{tot}}\mathbf{V}_{\mathrm{cm}}\gamma, \tag{40}$$

$$Q\ddot{\eta} = \sum_j m_j v'^2_{\mathbf{R},j} - (N_{\mathrm{f}}-3)k_{\mathrm{B}}T, \tag{41}$$

$$Q_\star\ddot{\eta}_\star = \sum_j m'_j v^2_{\mathbf{d},j} - N_{\mathrm{f}\star}k_{\mathrm{B}}T_\star, \tag{42}$$

$$W\ddot{\varepsilon} = a\sum_j (m_j v^2_{\mathbf{R},j} + m'_j v^2_{\mathbf{d},j}) + \sum_j (\mathbf{R}_j\cdot\mathbf{F}_{\mathbf{R},j} + \mathbf{d}_j\cdot\mathbf{F}_{\mathbf{d},j}) - 3PV, \tag{43}$$

where γ is the friction coefficient of the heat sink. The room-temperature thermostat is coupled to $N_{\mathrm{f}}-3$ degrees of freedom instead of N_{f}. The friction coefficient γ is chosen large enough to damp the center-of-mass motion down to a negligible contribution. The heat sink constitutes a further extension of the system and the energy E_{AH} [see Eq. (33)], that does not include the work $-\int dt\, M_{\mathrm{tot}}V^2_{\mathrm{cm}}\gamma$ exerted on the center of mass, is not exactly conserved anymore. Equations (36) to (43) generate a modified two-temperature isobaric–isothermal ensemble that we denote $NP(T,T_\star)$, where the second temperature refers to the auxiliary polarization variables.

In contrast to the system of Eqs. (25) to (31), the modified system of Eqs. (36) to (43) is irreversible. Alternative, fully reversible treatments could be devised. For example, one could replace the dissipative term in Eq. (40) by a chain of Nosé–Hoover thermostats.[75] As it will be shown in Sec. IV A, this is unimportant here because the total momentum is ''almost'' perfectly conserved by the numerical integration, and the introduction of the linear damping does not alter the precision of the simulation. In practice, the nonzero friction γ produces a very small work (less than 0.000 02 kcal/mol/ps on average). Therefore, the dissipative term has essentially no impact on the accuracy of the trajectory or on the conservation of the total energy.

III. COMPUTATIONAL DETAILS

The constant-temperature and constant-pressure molecular dynamics procedures described above has been implemented in the biomolecular program CHARMM.[79] To illustrate and test the present algorithm, a cubic system of 250 water molecules represented by the polarizable SPC (PSPC) model[61] was considered. The PSPC model is based on the original SPC (simple point charge) model.[7] It has the same tetrahedral-like geometry, with $\ell_{\mathrm{OH}}=1.0$ Å and $\theta_{\mathrm{HOH}}=109.47°$. It has a single polarizable site located on the oxygen atom, and hydrogen atoms are not polarizable. Both the molecular dipole and molecular polarizability correspond to the experimental gas-phase values, with μ_0 of 1.885 27 D and α of 1.44 Å^3. The nonpolar interactions are modeled using the usual Lennard-Jones 6–12 potential between each oxygen–oxygen pair. All the parameters of the model are given in Table I. Our own version of the PSPC model reproduces the polarizability by coupling a Drude particle to the oxygen site, with a harmonic spring of force constant k_{D} of 1000 kcal/mol/Å^2 and a positive charge $q_{\mathrm{D}}=\sqrt{\alpha k_{\mathrm{D}}}$, that is, 2.082 41 e. The total potential energy is

$$U(\{\mathbf{r}\}) = \sum_i \frac{1}{2}k_{\mathrm{D}}|\mathbf{r}_{\mathrm{O},i}-\mathbf{r}_{\mathrm{D},i}|^2 + \sum_{i,s}\sum_{j>i,t}\frac{q_{s,i}q_{t,j}}{|\mathbf{r}_{s,i}-\mathbf{r}_{t,j}|} + \sum_i\sum_{j>i}U_{\mathrm{LJ}}(|\mathbf{r}_{\mathrm{O},i}-\mathbf{r}_{\mathrm{O},j}|), \tag{44}$$

TABLE I. Parameters and dimer properties of the SPC (Ref. 7) and PSPC (Ref. 61) models. The components of the traceless quadrupole Q are defined with respect to the center-of-mass of the molecule, using the ∠HOH bisector as x axis, the H_1H_2 direction as y axis, and the perpendicular direction as z axis.

	Expt.	SPC[a]	PSPC[b]
ℓ_{OH} (Å)	0.9572[c]	1.0000	1.000 0
θ_{HOH} (°)	104.52[c]	109.47	109.47
q_O (e)		−0.82	−2.751 41
q_H (e)		0.41	0.334 50
q_D (e)			2.082 41
k_D (kcal/mol/Å^2)			1000
ϵ (kcal/mol)		0.1554	0.129 49
σ (Å)		3.1655	3.263 00
μ_0 (D)	1.85	2.274	1.855 27
Q_{xx} (DÅ)	−0.134[d]	−0.2938	−0.239 7
Q_{yy} (DÅ)	2.626[d]	2.1162	1.726 5
Q_{zz} (DÅ)	−2.493[d]	−1.8224	−1.486 8
α (Å^3)	1.44		1.44
U_d (kcal/mol)	−5.4[e]	−6.61	−4.29
d_d (Å)	2.98[e]	2.75	2.86
ϕ_d (°)	58±6[e]	22	19
μ_d (D)	2.643[e]	3.622	3.571

[a]From Ref. 7.
[b]From Ref. 61. The parameters q_D and k_D are specific to the Drude oscillator model and are not in the original reference.
[c]From Ref. 92.
[d]From Ref. 93.
[e]Dimer properties from Ref. 94: binding energy U_d, oxygen–oxygen distance d_d, acceptor angle ϕ_d, and total dipole μ_d.

where the labels s and t represent the four sites O, D, H_1, and H_2.

Molecular dynamics simulations at constant pressure were performed according to the three following procedures:

(1) *Traditional SCF regime*. At every time step, a Newton–Raphson energy minimization is performed to keep the massless Drude particles at their minimum-energy positions until the root-mean-square force on the oscillators is under 10^{-6} kcal/mol/Å. The nuclear motion is produced by Eqs. (36) to (43) in the special case where $\{m_i'=0\}$, $\{\mathbf{F}_{\mathbf{d},i}=0\}$, $P=1$ atm, and $T_\star=0$.
(2) *Cold Drude oscillators regime*. Trajectories are generated in the $NP(T,T_\star)$ ensemble using Eqs. (36) to (43) with $P=1$ atm, $T=298.15$ K, and $T_\star=1$ K.
(3) *Thermalized Drude oscillators regime, $NP(T,T)$ ensemble*. Trajectories are generated in the $NP(T=T_\star)$ ensemble using Eqs. (36) to (43) with $P=1$ atm and $T=T_\star=298.15$ K.

Each molecule has 6 degrees of freedom for the nuclei and 3 for the Drude oscillator, thus $N_f=6N_{mol}$ and $N_{f\star}=3N_{mol}$. Inertia parameters Q and W are set using both τ and τ_ε equal to 0.1 ps, and using $N_{f\varepsilon}=N_f$ for the SCF and the cold Drude oscillators simulations, but $N_{f\varepsilon}=N_f+N_{f\star}$ for the thermalized Drude oscillators simulations. The residual center-of-mass motion is dissipated using $\gamma=10$ ps^{-1}, even for the SCF simulations, where the flying ice cube problem is very unlikely. The extended dynamics simulations are done for various m_D values: 0.8, 0.4, 0.2, and 0.1 amu. The period of free oscillation of the Drude particles is $2\pi\sqrt{m_D/k_D}$, corresponding to 8.69 fs for a mass of 0.8 amu and decreasing as $\sqrt{m_D}$ for other masses. The characteristic response time of the second thermostat, $\tau_\star$, should be short enough to follow this fast motion. For the cold Drude oscillators simulations, $\tau_\star$ is set to 7.07 fs for $m_D=0.8$ amu, 5.00 fs for $m_D=0.4$ amu, 3.54 fs for $m_D=0.2$ amu, and 2.50 fs for $m_D=0.1$ amu. For the thermalized Drude oscillators simulations, five-time-longer and five-time-shorter time scales are tested as well: 35.36, 7.07, and 1.41 fs for $m_D=0.8$ amu, and so on for other m_D values.

The motion was integrated with time steps Δt of 0.5, 1.0, and 2.0 fs, using the multistep thermostat integration with $n_c=100$. Drude particles having a mass of 0.4 amu are oscillating at a frequency $\omega=\sqrt{k_D/m_D}$, corresponding to about 1 fs^{-1}. Given that $\omega\Delta t$ should be small compared to 1 in order for the motion of the oscillator to be precisely integrated,[67] none of these time steps would be recommendable for conventional molecular dynamics. The internal water geometry was constrained using the SHAKE/Roll and RATTLE/Roll procedures.[71] The electrostatic interactions were calculated with the particle-mesh Ewald summation[80] and a 9 Å cutoff for the Lennard-Jones (LJ) interaction.

Each box was simulated for 150 ps and its properties were extracted from the last 100 ps. The following properties are accumulated: the average potential energy Δu, the average molecular volume $\langle v\rangle$, the pair distribution functions $g_{OO}(r)$, $g_{OH}(r)$, and $g_{HH}(r)$, and the average molecular dipole $\langle\mu\rangle$. The average net gain of potential energy Δu upon formation of the dense system is

$$\Delta u=[\langle u_{liq}\rangle-\langle u_{gas}\rangle]=[\langle u_{liq}\rangle-\tfrac{3}{2}k_BT_\star] \tag{45}$$

and is related to the vaporization enthalpy Δh

$$\Delta h=k_BT-\langle\Delta u\rangle. \tag{46}$$

It should be noted that, even though the water molecules themselves may be rigid, the thermal contribution from the Drude oscillators to the total potential energy, $\frac{3}{2}k_BT_\star$, must be rigorously subtracted in an extended Lagrangian simulation (though this number is small if $T_\star\approx1$). The self-diffusion constant D and the static dielectric constant ϵ were computed from the last 100 ps of ten independent simulations of 150 ps, using the expressions[81,82]

$$D=\lim_{t\to\infty}\frac{1}{6t}\left\langle\frac{1}{N}\sum_{i=1}^{N}|\mathbf{r}_{O,i}(t)-\mathbf{r}_{O,i}(0)|^2\right\rangle, \tag{47}$$

and

$$\epsilon=\epsilon_\infty+\frac{4\pi}{3\langle V\rangle k_BT}(\langle\mathbf{M}^2\rangle-\langle\mathbf{M}\rangle^2), \tag{48}$$

where $\langle V\rangle$ is the average volume of the box and $\mathbf{M}$ is the total dipole moment of the box. For thermalized Drude oscillators, $\epsilon_\infty=1$, because all electrostatic response is included in $\langle\mathbf{M}^2\rangle$. In the SCF regime, or whenever $T_\star$ is very low, ϵ_∞ can be estimated from the Clausius–Mossotti equation

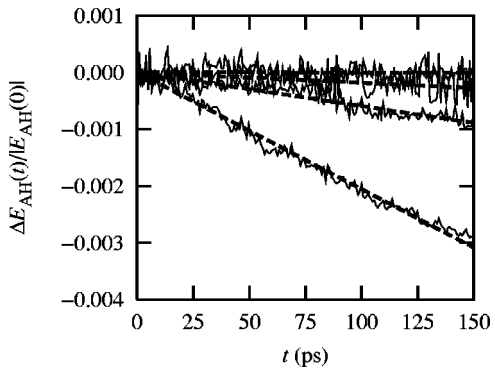

FIG. 1. Relative deviation of the extended energy for $T_\star = 1$ K and $T_\star = 0$ K (SCF) simulations (with a 1.0 fs time step). A larger m_D creates a larger downward energy drift: -0.0338 kcal/mol/ps for $m_D = 0.8$ amu, -0.0098 kcal/mol/ps for $m_D = 0.4$ amu, -0.0031 kcal/mol/ps for $m_D = 0.2$ amu, and no noticeable drift for $m_D = 0$ amu (SCF).

$$\frac{\epsilon_\infty - 1}{\epsilon_\infty + 2} = \frac{4\pi}{3}\frac{\alpha}{v}. \tag{49}$$

For $\alpha = 1.44$ Å^3, we get $\epsilon_\infty = 1.75$ if $v = 30$ Å^3 (the experimental molecular volume) and $\epsilon_\infty = 1.70$ if $v = 32$ Å^3 (the molecular volume of the PSPC model, as it will be shown later). The uncertainty on D and ϵ was estimated from the spread over the ten simulations.

IV. RESULTS AND DISCUSSION

A. Numerical precision and stability

The stability and accuracy of the trajectories generated according to the SCF procedure is first examined. The result from those trajectories is then used as reference to assess the correctness of the trajectories generated with extended dynamics simulations with "cold" and thermalized ("hot") Drude oscillators. The trajectories generated with the SCF procedure are stable for all three time-step values (0.5, 1.0, and 2.0 fs). For $\Delta t = 0.5$ and 1.0 fs, the total extended energy E_{AH} of Eq. (33) has no noticeable drift (see Fig. 1 for $\Delta t = 1.0$ fs). For $\Delta t = 2.0$ fs, E_{AH} is very slowly drifting down, at a rate of -0.0009 kcal/mol/ps. This excellent energy conservation reflects the fact that the massless Drude particles follow adiabatically according to the motion of the atoms. The simulations are stable because the very high-frequency motion of the light Drude particles is effectively not present in the SCF trajectories. The convergence of the SCF procedure is very closely related to the number of iterations of the Newton–Raphson energy minimization.[79] For each molecular dynamics integration time step, the SCF procedure requires about 16 iterations to converge to the desired criterion ($F_{rms} < 10^{-6}$ kcal/mol/Å). This procedure yields a precise SCF trajectory but is computationally expensive because each time step requires 16 evaluations of the atomic forces. It may be tempting to reduce the computational cost of SCF by simply using a less stringent convergence criterion. But, whether the properties of the system are affected by an imprecise SCF scheme is unclear. Test simulations using a convergence criterion of $F_{rms} < 10^{-4}$ kcal/mol/Å give the same liquid properties with 12 iterations, but exhibit a somewhat faster downward drift in E_{AH} (-0.0215 kcal/mol/ps for $\Delta t = 2.0$ fs). Test simulations using $F_{rms} < 10^{-2}$ kcal/mol/Å require only 7 iterations every step, but exhibit an unacceptable energy drift of -6.53 kcal/mol/ps. This gives rise to spurious dragging forces that lower the self-diffusion constant and distort the liquid structure. In a recent study, Yu *et al.*[58] have used a very tolerant iteration scheme that requires only 2 or 3 iterations for every time step. Our own test simulations indicate that propagating a trajectory with a convergence criterion that requires only 3 iterations, that is, $F_{rms} < 1$ kcal/mol/Å, yields a liquid that is significantly more dense and a self-diffusion constant that is about four times smaller than the true SCF value. Our tests indicate that iterating at least until $F_{rms} < 10^{-4}$ kcal/mol/Å guarantees that the Drude particles have a truly SCF motion. We use $F_{rms} < 10^{-6}$ kcal/mol/Å as a precaution.

Extended dynamics simulations, which treat the Drude particles as simple classical degrees of freedom, require only a single evaluation of the forces per time step and are, thus, much more efficient than the slow SCF procedure. Overall, simulations generated with cold Drude oscillators ($T_\star = 1$ K) appear to be more stable and to conserve energy better than simulations with hot Drude oscillators ($T_\star = 298.15$ K). Using a time step of 0.5 fs with either $T_\star = 1$ K or $T_\star = 298.15$ K gives stable trajectories for all four values of the mass assigned to the Drude particles. But, when a time step of 1.0 fs is used, simulations with $T_\star = 298.15$ K are unstable for $m_D = 0.1$ and 0.2 amu, whereas simulations with $T_\star = 1$ K are unstable only for $m_D = 0.1$ amu. Using a time step of 2.0 fs, simulations with $T_\star = 1$ K are stable for $m_D = 0.8$ amu, whereas no simulations with $T_\star = 298.15$ K are stable. For stable simulations, the energy E_{AH} is well conserved for $T_\star = 1$ K (see Fig. 1 for $\Delta t = 1.0$ fs). The energy drift is slow for $m_D = 0.8$ amu and becomes even slower as m_D is decreased. In contrast, the energy conservation is much poorer for $T_\star = 298.15$ K. And, although it is improved by using a five-times shorter relaxation time for the $T_\star$ thermostat (that is, $\tau_\star = 1.41$ fs for $m_D = 0.8$ amu, and so on for other m_D values), the energy drift is about an order of magnitude larger for $T_\star = 298.15$ K than it is for $T_\star = 1$ K. With $m_D = 0.8$ amu, using $\tau_\star = 35.36$ or even 7.07 fs creates spurious temperature oscillations. These are clear indications that, for a given Drude oscillator mass and given time step, the trajectories are more precisely integrated with $T_\star = 1$ K than with $T_\star = 298.15$ K. The kinetic temperatures,

$$T(t) \equiv \sum_j m_j v'^2_{\mathbf{R},j} / (N_f - 3) k_B, \tag{50}$$

and

$$T_\star(t) \equiv \sum_j m'_j v^2_{\mathbf{d},j} / N_{f\star} k_B, \tag{51}$$

are correctly regulated and $\langle T(t) \rangle = 298.15$ K and $\langle T_\star(t) \rangle = 1$ K within statistical error. As shown in Fig. 2, the temperature $T(t)$ exhibits canonical fluctuations and is distributed according to a Gaussian with a standard deviation $\sigma = 10.9$ K, as expected for a finite system in the canonical

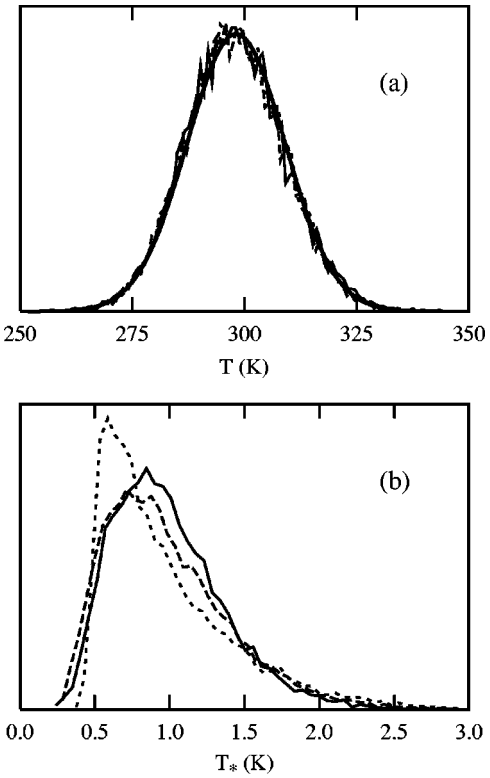

FIG. 2. Temperature distributions (a) for T and (b) for $T_\star$ for $m_D=0.2$ (solid lines), $m_D=0.4$ (dashed lines), and $m_D=0.8$ (dotted lines). The smooth solid line in (a) is the expected temperature distribution in the canonical ensemble for 1497 degrees of freedom.

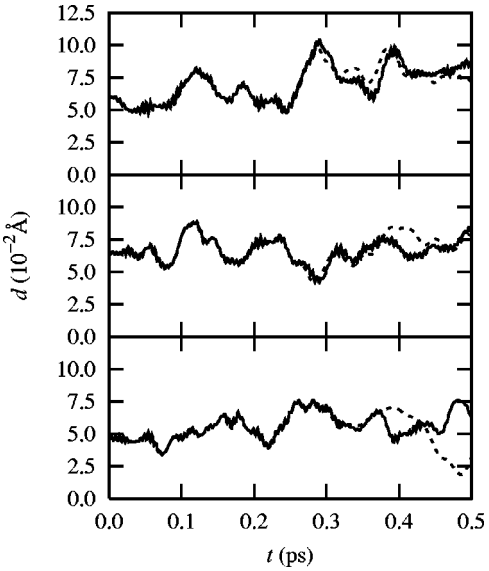

FIG. 3. Comparison of the trajectories of three Drude particles for $m_D=0.4$ amu and $T_\star=1$ K (solid lines), and SCF regime (dashed lines).

ensemble[83] [$\sigma^2=2\langle T\rangle^2/(N_f-3)$, with $N_f=6\times250$]. In contrast, fluctuations in the temperature $T_\star$ are not distributed according to a Gaussian. As seen in Fig. 2, the distribution is asymmetric and skewed toward the low temperatures. This skewness reflects the small but steady nonequilibrium heat flow in the system. It is more pronounced for a larger value of m_D, that is, when the kinetic coupling between the Drude and the nuclear degrees of freedom is stronger. Nonetheless, this behavior does not appear to have any consequences on the molecular motion, which obeys the canonical distribution at the correct temperature.

Although the total momentum is rigorously conserved by Eqs. (25) to (31), a spurious translation of the center of mass of the system does arise slowly after some time due to an accumulation of small numerical errors. Preliminary tests show that the center-of-mass can develop a net translation of about 0.03 Å/ps on average after a trajectory of 100 ps (data not shown). From Eq. (35), the time scale for the onset of the flying ice cube artifact can be estimated from $1/|\langle\dot{\eta}\rangle|$, giving about 4 ns for $m_D=0.8$ amu, 19 ns for $m_D=0.4$ amu, and longer for $m_D=0.2$ and 0.0 amu. These time scales are sufficiently long to allow Eqs. (25) to (31) to be used directly for simulations where rigorously reversible dynamics is required and avoid the flying ice cube artifact. Nevertheless, although the errors are very small for the current simulations of a simple bulk liquid, the problem may become much more acute in the case of large and complex biomolecular systems. To completely avoid any acceleration of the center of mass, the system was propagated using Eqs. (36) to (43), in which a small irreversible damping was applied to the global translation of the system. Because the original equations conserve the total momentum almost perfectly, the amount of energy dissipated by the irreversible damping is nearly negligible (less than 0.000 02 kcal/mol/ps on average).

To illustrate more directly the correspondence between the cold Drude oscillators simulations and the SCF simulations, the time course of the oscillators of three randomly picked water molecules are compared in Fig. 3. Using the same initial coordinates and velocities for the nuclei, both simulation methods produce nearly identical trajectories for the first 0.3 ps, after which the chaotic nature of the motion in the liquid takes over and the trajectories diverge rapidly from one another. This time scale is comparable to the decay time of the velocity autocorrelation function, suggesting that dynamical properties should be simulated precisely.

As a side issue, one may note that the kinetic coupling between the high-frequency Drude oscillators and the remaining degrees of freedom in the system is very weak. Thermalization of the motion of the Drude oscillators can be achieved from this weak coupling only, but it is significantly accelerated with a coupling to a separate, fast-reacting thermostat. In the simulations with thermalized Drude oscillators, the second thermostat at $T_\star=298.15$ K allows a rapid equipartition of the energy, whereas a few tens of picoseconds were needed in the simulations of van Belle *et al.* based on an extended dynamics scheme with point dipoles.[66] In those simulations a dipole inertia factor of 0.5 amu/e^2, equivalent to a mass of $m_D=2.168$ amu, was used. The thermalization time grows as the inertia of the dipoles is decreased. For instance, our own test simulations without a separate thermostat on the Drude oscillators show that oscillators with $m_D=0.4$ amu require as much as 150 ps to fully thermalize. This is a very long simulation time during which the thermodynamic properties are unreliable.

TABLE II. Liquid properties for the PSPC water model for cold, thermalized, and SCF Drude oscillators, compared with SPC and experimental properties. Dashes indicate unstable simulations.

$T_\star$ (K)	Δt (fs)	m_D (amu)	Δu (kcal/mol)	$\langle v \rangle$ (Å^3)	$\langle \mu \rangle$ (D)	D (10^{-5} cm^2/s)	ϵ
1.00	0.5	0.8	−7.94	32.13	2.714	3.98±0.06	195±30
		0.4	−7.94	32.13	2.714	3.91±0.09	175±30
		0.2	−7.95	32.11	2.715	3.87±0.07	195±30
		0.1	−7.95	32.12	2.715	3.93±0.06	205±30
	1.0	0.8	−7.94	32.13	2.714	3.93±0.06	225±30
		0.4	−7.94	32.12	2.714	3.97±0.08	185±30
		0.2	−7.94	32.13	2.714	3.96±0.10	170±30
		0.1	⋯				
	2.0	0.8	−7.92	32.14	2.712	4.03±0.07	210±30
		0.4	⋯				
		0.2	⋯				
		0.1	⋯				
298.15	0.5	0.8	−7.95	31.88	2.744		
		0.4	−7.93	31.90	2.745		
		0.2	−7.88	31.61	2.752		
		0.1	−7.74	31.13	2.761		
	1.0	0.8	−7.86	31.56	2.750		
		0.4	−7.71	31.03	2.760		
		0.2	⋯				
		0.1	⋯				
SCF	1.0	0.0	−7.94	32.14	2.714	3.86±0.05	190±30
	2.0	0.0	−7.92	32.16	2.712	3.98±0.06	195±30
Ahlström *et al.* (Ref. 61)[a]			−9.08	29.92	2.9	2.0±0.2	
van Belle *et al.* (Ref. 65)[a]			−9.11	29.92	2.8	2.4±0.2	
SPC[b]			−9.79	31.2	2.274	3.91±0.04	73±10
Experiment			−9.92[c]	30.0[d]		2.3[e]	78.4[f]

[a]Constant-volume simulations.
[b]Liquid properties computed from 20 simulations of 250 molecules in the isothermal–isobaric ensemble, using particle-mesh Ewald and a 9 Å Lennard-Jones cutoff.
[c]From the experimental vaporization enthalpy $\Delta h = 10.52$ kcal/mol (Ref. 95) using $\Delta h = k_B T - \Delta u$.
[d]Corresponding to 0.997 g/cm^3.
[e]From Ref. 96.
[f]From Ref. 88.

B. Average properties of the liquid

Table II summarizes the average properties of the liquid obtained with the various simulation procedures. In the following, the SCF simulations are used as a reference to assess the accuracy of the extended dynamics trajectories. It is observed that the simulations with the cold Drude oscillators give consistent results for all the values of the mass m_D that were tested. For a given time step, Δu, $\langle v \rangle$, $\langle \mu \rangle$, and the $g(r)$ distribution functions (see Fig. 4) are all within the statistical errors. Most importantly, they are very close to the properties calculated from the trajectories generated according to the SCF procedure. The time step seems to have a very small systematic effect on the properties, but the effect is probably not specific to the motion of the Drude oscillators because it is independent of m_D and is noticeable for the SCF values as well. The self-diffusion constant D and the dielectric constant ϵ are close to the SCF values as well—within the estimated uncertainties. Figure 5 shows that the histograms of the induced dipole for the simulations generated with cold Drude oscillators superimpose to the SCF results and are independent of the mass attributed to the Drude particles.

It is clear that the simulations generated with thermalized Drude oscillators exhibit some systematic deviations relative to those generated with SCF or with the cold Drude oscillators. In particular, there is a slight increase in the liquid density and of the average molecular dipole. This is caused by the presence of the small additional cohesion interaction arising from (classical) dipole–dipole correlations, given to lowest order term in Eq. (14). Furthermore, Fig. 5 shows that the $T_\star = 298.15$ K simulations exhibit a spurious enhancement of the dipole fluctuations if the mass of the Drude particle becomes too small. This observation is in accord with previous analysis which shows that the relative error on the mean-squared displacement of an oscillator of frequency ω simulated with a velocity-Verlet algorithm varies as $\omega^2 \Delta t^2$.[67] As a consequence of the inaccurate integration of the high-frequency motion of the Drude oscillators, the average equilibrium thermodynamics properties now exhibit an unphysical dependence upon the choice of mass attributed to the Drude particles. As m_D decreases, $\langle \mu \rangle$ slightly increases, $\langle v \rangle$ decreases, and Δu is becoming less negative. In contrast, the results from the cold Drude oscillators simulations do not vary as m_D is decreased. This strongly indi-

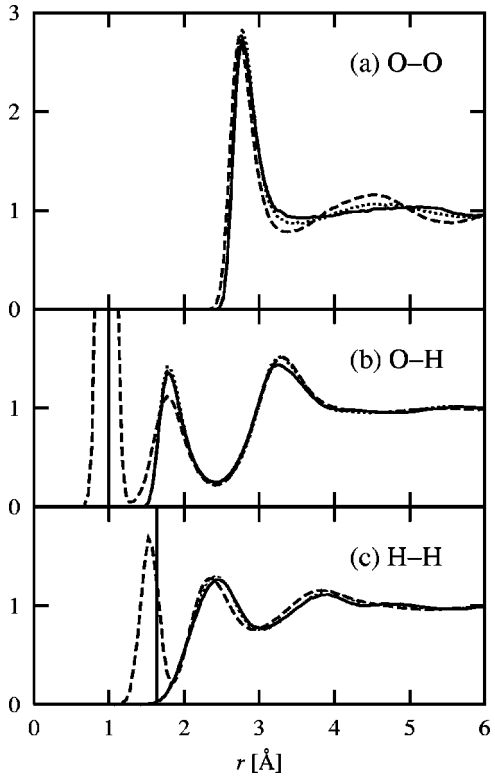

FIG. 4. (a) Oxygen–oxygen; (b) oxygen–hydrogen; and (c) hydrogen–hydrogen radial distribution functions for PSPC model (solid lines), compared to SPC distributions (dotted lines) and experimental distributions from Soper *et al.* (Ref. 97) (dashed lines). Only the PSPC distributions obtained with $T_\star = 0$ K with $\Delta t = 2.0$ fs are shown, but $T_\star = 1$ K gives indistinguishable curves.

cates that generating trajectories with cold Drude oscillators should be the method of choice to simulate such models.

It is of interest to compare the present results with those of previous simulations and with experimental data. The PSPC model was previously simulated using a relatively tolerant SCF procedure by Ahlström *et al.*,[61] and using an extended dynamics algorithm by van Belle *et al.*[65] The main results from those simulations are included at the bottom of Table II. The results of Ahlström *et al.* and van Belle *et al.* are relatively uniform, but show significant discrepancies with the present results, particularly concerning the enthalpy, the average density, and the self-diffusion constant. It is unlikely that these discrepancies are due to the fact that the original point dipole of the PSPC model was replaced by a Drude oscillator, because for the simulations at $T_\star = 298.15$ K the Drude particles are almost never displaced by more than 0.2 Å (see Fig. 5). Even at this separation, the point dipole remains a good approximation. The discrepancies are most probably due to the fact that the present work uses a constant-pressure algorithm, whereas the previous simulations were performed at a constant volume corresponding to the experimental density of water. In addition, a PME summation was used here instead of a screening and cutoff scheme.[61,65] To further compare with the results of Ahlström *et al.* and van Belle *et al.*, additional $T_\star = 298.15$ K simulations were done at constant volume [using Eqs. (36) to (43) with an infinite W and assuming a constant density of $1\ \mathrm{g/cm^3}$]. At constant volume, with $m_\mathrm{D} = 1.0$ amu and using the Ewald summation, we get $\Delta u = -7.41$ kcal/mol. The remaining discrepancy with the original results $[-9.08 \pm 0.07$ (Ref. 61) and -9.11 ± 0.05 kcal/mol (Ref. 65)] is caused by the differences in the treatment of the electrostatic interactions. Additional test simulations using an electrostatic screening and cutoff scheme instead of PME reproduces the previous results for the enthalpy.[61,65] The present constant-pressure PME simulations show that the true liquid density of the PSPC model is, in fact, too low and that the average potential energy Δu is about 2 kcal/mol off compared to experiments. Last, the present simulations show that the dielectric constant is on the order of 200. This high dielectric constant is consistent with the average molecular dipole of 2.71 D observed in the simulations. According to a trend observed for a number of simple water models similar to PSPC,[84–87] the average molecular dipole in the liquid should be around 2.4 to 2.6 D to reproduce the correct dielectric constant of 78.4.[88] The present analysis is not meant to be a criticism of the previous efforts to design and simulate the PSPC model more than a decade ago.[61,65] Nonetheless, it highlights the general importance of avoiding truncated electrostatics with cutoff schemes in simulations of polar liquids, and the difficulties in designing and parametrizing a simple computational model that reproduces the properties of liquid water accurately.

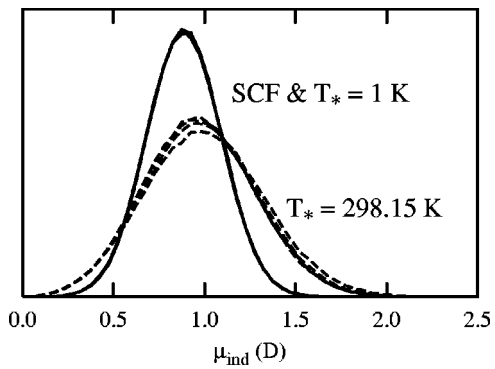

FIG. 5. Induced dipole histograms for SCF simulations with $\Delta t = 1.0$ fs (solid line); $T_\star = 1$ K simulations with $\Delta t = 1.0$ fs and $m_\mathrm{D} = 0.8$, 0.4, and 0.2 amu (three curves in solid lines, indistinguishable from the SCF curve); and $T_\star = 298.15$ K simulations with $\Delta t = 0.5$ fs (dashed lines). Dashed histograms get lower and wider as m_D decreases from 0.8, 0.4, 0.2, to 0.1 amu. It shows that, for room-temperature Drude oscillators, both average-induced dipole and the dipole fluctuations have unphysical dependences on m_D. For $T_\star = 1$ K simulations, the induced dipoles are rarely larger than 1.5 D, corresponding to an actual Drude displacement of about 0.15 Å.

V. SUMMARY

We have presented a general polarizable model based on Drude oscillators and demonstrated that the SCF motion of the Drude oscillators can be efficiently and accurately simulated with an extended molecular dynamics simulation procedure keeping the polarization variables at low temperature. This is done by using two separate thermostats for the ''atomic'' and ''dipolar'' motions of the polarizable atoms. An algorithm to generate molecular dynamics trajectories in this modified two-temperature isobaric–isothermal

$NP(T,T_\star)$ ensemble was described. Tests demonstrated that this is the most advantageous approach for molecular dynamics simulations of polarizable model based on classical Drude oscillators. The traditional SCF procedure, in which the Drude particles are kept at the minimum of their local energy surface, is at least one order of magnitude more expensive computationally than this algorithm. An alternative extended dynamical approach, in which the Drude particles are allowed to equilibrate thermally with the nuclei at room temperature, was found to yield some liquid properties inaccurately and was also less stable numerically.

The present results show that simulations in the $NP(T,T_\star)$ ensemble have a clear advantage over $NP(T,0)$ and $NP(T,T)$ simulations. With separate atomic and dipolar thermostatting, the particles are kept in a regime where the stiff Drude oscillator forces counterbalance the induction forces and leave a slowly varying net force that can be integrated using a reasonably large time step. A 2.0 fs time step can safely be used with $m_D=0.8$ amu and retain accurate thermodynamic as well as dynamical properties. Molecular dynamics with cold Drude oscillators ($T_\star=1$ K) is more than an order of magnitude more efficient than the SCF regime but produces nearly equivalent liquid properties. The modified isobaric–isothermal $NP(T,T_\star)$ method is more efficient than molecular dynamics with thermalized Drude oscillators, that requires a smaller time step to integrate the motion of the hot Drude oscillators with the same accuracy. It is preferable as well, because the thermal fluctuations of the Drude oscillators have a small but undesirable cohesive effect on the liquid.

The Drude oscillator model has several advantages over a point–dipole model. It gives an intuitive physical picture in terms of a displacement of the electronic distribution. The auxiliary particle can inherit any of the properties of a model atom: dipole screening could be implicitly incorporated using charge screening for the Drude particles and the nuclei, and dispersion and repulsion effects could be extended to the dipole using a shallow Lennard-Jones potential on the Drude particles, thus allowing mechanical polarizability.[17] Representing a dipole as two point charges allows any pre-existing, charge-based, implementation of the particle-mesh Ewald summation[80] to be used. Last, because the dipole is not pointlike, the model is able to represent an actual charge delocalization without the need of additional nonatomic sites.

As for any explicitly polarizable model, the drawback is that the system has additional degrees of freedom, thereby increasing the computational cost of the simulation. For pure water, having additional auxiliary particles only on the oxygen atoms makes a standard $O(N\log N)$ computation of the atomic forces is about 40% more expensive for a three-site model like the one used in this work, and about 30% for a four-site model. Therefore, trajectories generated in the two-temperatures isobaric-isothermal $NP(T,T_\star)$ ensemble are essentially equivalent to those generated according to the traditional SCF procedure at a fraction of the cost.

In the near future, efforts will be dedicated to the parametrization of a polarizable water model based on classical Drude oscillators that correctly reproduces all the essential properties of the liquid phase while improving the accuracy of the microscopic water–water interactions compared to the nonpolarizable models. Because polarizability is essential for a better understanding of the affinity and coordination of small charged ligands to protein or nucleic acid molecules,[15] the following logical step will be to get similar polarizable models to improve the microscopic representation of ion–water and ion–protein interactions. The present scheme will be the basis for an explicitly polarizable force field for molecular dynamics of proteins and nucleic acids.

ACKNOWLEDGMENTS

Helpful discussions with Alexander D. MacKerell, Jr., Bruce J. Berne, and Mark E. Tuckerman are gratefully acknowledged. G.L. is grateful to Alain Caillé for his support. This work was supported by Grant No. 0110847 from the National Science Foundation.

APPENDIX A: SELF-CONSISTENT EQUATIONS FOR INDUCED POLARIZATION

For unscreened Coulomb interactions

$$U_{\mathrm{elec}}=\sum_i\sum_{j>i}\left[\frac{(q_i-q_{\mathrm{D},i})(q_j-q_{\mathrm{D},j})}{|\mathbf{r}_i-\mathbf{r}_j|}+\frac{(q_i-q_{\mathrm{D},i})q_{\mathrm{D},j}}{|\mathbf{r}_i-\mathbf{r}_j-\mathbf{d}_j|}+\frac{q_{\mathrm{D},i}(q_j-q_{\mathrm{D},j})}{|\mathbf{r}_i+\mathbf{d}_i-\mathbf{r}_j|}+\frac{q_{\mathrm{D},i}q_{\mathrm{D},j}}{|\mathbf{r}_i+\mathbf{d}_i-\mathbf{r}_j-\mathbf{d}_j|}\right]. \tag{A1}$$

Assuming that the **d**'s are small, all terms can be expanded into charge–charge, charge–dipole, and dipole–dipole contributions

$$U_{\mathrm{elec}}\simeq\sum_i\sum_{j>i}\left[\frac{q_iq_j}{r_{ij}}+(q_{\mathrm{D},i}\mathbf{d}_iq_j-q_iq_{\mathrm{D},j}\mathbf{d}_j)\cdot\boldsymbol{\nabla}_i\left(\frac{1}{r_{ij}}\right)-q_{\mathrm{D},i}\mathbf{d}_iq_{\mathrm{D},j}\mathbf{d}_j:\boldsymbol{\nabla}_i\boldsymbol{\nabla}_i\left(\frac{1}{r_{ij}}\right)\right]. \tag{A2}$$

All gradients have been converted to $\boldsymbol{\nabla}_i\equiv\partial/\partial\mathbf{r}_i$. Condition (4) of the text now reads

$$k_{\mathrm{D}}\mathbf{d}_k=\sum_{j\neq k}\left[-q_{\mathrm{D},k}q_j\boldsymbol{\nabla}_k\left(\frac{1}{r_{kj}}\right)+q_{\mathrm{D},k}q_{\mathrm{D},j}\mathbf{d}_j\cdot\boldsymbol{\nabla}_k\boldsymbol{\nabla}_k\left(\frac{1}{r_{kj}}\right)\right]. \tag{A3}$$

With $\boldsymbol{\mu}_k=q_{\mathrm{D},k}\mathbf{d}_k$ and $\alpha_k=q_{\mathrm{D},k}^2/k_{\mathrm{D}}$, these are Eqs. (6) of the text.

APPENDIX B: EFFECTIVE FIELD FOR THERMALIZED DRUDE OSCILLATORS

With $\boldsymbol{\mu}_i=q_{\mathrm{D},i}\mathbf{d}_i$, and because only U_{self} and U_{elec} depend on the **d**'s

$$\delta\mathbf{d}_i\cdot\frac{\partial^2 U}{\partial\mathbf{d}_i\partial\mathbf{d}_j}\cdot\delta\mathbf{d}_j=\delta\boldsymbol{\mu}_i\cdot\left(\frac{\partial^2 U_{\rm self}}{\partial\boldsymbol{\mu}_i\partial\boldsymbol{\mu}_j}+\frac{\partial^2 U_{\rm elec}}{\partial\boldsymbol{\mu}_i\partial\boldsymbol{\mu}_j}\right)\cdot\delta\boldsymbol{\mu}_j\,. \tag{B1}$$

With $\alpha_i=q_{{\rm D},i}^2/k_{\rm D}$

$$\frac{\partial^2 U_{\rm self}}{\partial\boldsymbol{\mu}_i\partial\boldsymbol{\mu}_j}=\delta_{ij}\frac{\mathbf{1}}{\alpha_i}\equiv\mathbf{A}_{ij}^{-1}, \tag{B2}$$

where $\mathbf{1}$ is the 3×3 identity matrix. From Eq. (A2) in the point–dipole approximation

$$\frac{\partial^2 U_{\rm elec}}{\partial\boldsymbol{\mu}_i\partial\boldsymbol{\mu}_j}=-\boldsymbol{\nabla}_i\boldsymbol{\nabla}_i\left(\frac{1}{r_{ij}}\right)\equiv-\mathbf{T}_{ij}\,. \tag{B3}$$

Integrating over point–dipole fluctuations $\{\delta\boldsymbol{\mu}\}$ instead of displacement fluctuations $\{\delta\mathbf{d}\}$, the correction factor on the right-hand-side of Eq. (13) is

$$\frac{\int d\{\delta\boldsymbol{\mu}\}\Pi_{ij}e^{-(1/2)\,\beta\delta\boldsymbol{\mu}_i\cdot(\mathbf{A}_{ij}^{-1}-\mathbf{T}_{ij})\cdot\delta\boldsymbol{\mu}_j}}{\int d\{\delta\boldsymbol{\mu}\}\Pi_{ij}e^{-(1/2)\,\beta\delta\boldsymbol{\mu}_i\cdot\mathbf{A}_{ij}^{-1}\cdot\delta\boldsymbol{\mu}_j}}\equiv\left\langle\prod_{ij}\,e^{(1/2)\,\beta\delta\boldsymbol{\mu}_i\cdot\mathbf{T}_{ij}\cdot\delta\boldsymbol{\mu}_j}\right\rangle, \tag{B4}$$

where $\langle\ldots\rangle$ is an average over the thermal fluctuations of noninteracting dipoles. The average is expanded as a moment series

$$\left\langle\prod_{ij}\,e^{(1/2)\,\beta\delta\boldsymbol{\mu}_i\cdot\mathbf{T}_{ij}\cdot\delta\boldsymbol{\mu}_j}\right\rangle=1+\frac{\beta}{2}\sum_{ij}\,\mathbf{T}_{ij}\cdot\langle\delta\boldsymbol{\mu}_i\delta\boldsymbol{\mu}_j\rangle+\frac{1}{2}\left(\frac{\beta}{2}\right)^2\sum_{ijkl}\,\mathbf{T}_{ij}\mathbf{T}_{kl}\cdot\langle\delta\boldsymbol{\mu}_i\delta\boldsymbol{\mu}_j\delta\boldsymbol{\mu}_k\delta\boldsymbol{\mu}_l\rangle+\cdots. \tag{B5}$$

The two-point correlation functions are explicitly integrated

$$\langle\delta\boldsymbol{\mu}_i\delta\boldsymbol{\mu}_j\rangle=\frac{\int d\{\delta\boldsymbol{\mu}\}\Pi_{kl}\delta\boldsymbol{\mu}_i\delta\boldsymbol{\mu}_j e^{-(1/2)\,\beta\delta\boldsymbol{\mu}_k\cdot\mathbf{A}_{kl}^{-1}\cdot\delta\boldsymbol{\mu}_l}}{\int d\{\delta\boldsymbol{\mu}\}\Pi_{kl}e^{-(1/2)\,\beta\delta\boldsymbol{\mu}_k\cdot\mathbf{A}_{kl}^{-1}\cdot\delta\boldsymbol{\mu}_l}}=\frac{1}{\beta}\mathbf{A}_{ij}\,. \tag{B6}$$

From Wick's theorem (e.g., see Ref. 89), the four-point correlation functions are written as sums of two-point correlation functions

$$\langle\delta\boldsymbol{\mu}_i\delta\boldsymbol{\mu}_j\delta\boldsymbol{\mu}_k\delta\boldsymbol{\mu}_l\rangle=\frac{1}{\beta^2}(\mathbf{A}_{ij}\mathbf{A}_{kl}+\mathbf{A}_{ik}\mathbf{A}_{jl}+\mathbf{A}_{il}\mathbf{A}_{jk}). \tag{B7}$$

Because $\mathbf{T}_{ij}=\mathbf{0}$ for $i=j$ and $\mathbf{A}_{ij}=\mathbf{0}$ for $i\neq j$, the first term of Eq. (B5) is

$$\frac{\beta}{2}\sum_{ij}\,\mathbf{T}_{ij}\cdot\langle\delta\boldsymbol{\mu}_i\delta\boldsymbol{\mu}_j\rangle=\frac{1}{2}\sum_{ij}\,\mathbf{T}_{ij}\cdot\mathbf{A}_{ij}=0, \tag{B8}$$

and the second term is

$$\frac{1}{2}\left(\frac{\beta}{2}\right)^2\sum_{ijkl}\,\mathbf{T}_{ij}\mathbf{T}_{kl}\cdot\langle\delta\boldsymbol{\mu}_i\delta\boldsymbol{\mu}_j\delta\boldsymbol{\mu}_k\delta\boldsymbol{\mu}_l\rangle=\frac{1}{8}\sum_{ijkl}\,\mathbf{T}_{ij}\mathbf{T}_{kl}\cdot(\mathbf{A}_{ij}\mathbf{A}_{kl}+\mathbf{A}_{ik}\mathbf{A}_{jl}+\mathbf{A}_{il}\mathbf{A}_{jk})=\frac{1}{4}\sum_{ijkl}\,\mathbf{T}_{ij}\mathbf{T}_{kl}\cdot\mathbf{A}_{ik}\mathbf{A}_{jl}\,. \tag{B9}$$

Because $\mathbf{T}_{ij}=(3\hat{\mathbf{r}}_{ij}\hat{\mathbf{r}}_{ij}-\mathbf{1})/r_{ij}^3$,

$$\frac{1}{4}\sum_{ijkl}\,\mathbf{T}_{ij}\mathbf{T}_{kl}\cdot\mathbf{A}_{ik}\mathbf{A}_{jl}=\frac{3}{2}\sum_{ij}\,\frac{\alpha_i\alpha_j}{r_{ij}^6}, \tag{B10}$$

and

$$\left\langle\prod_{ij}\,e^{1/2\,\beta\delta\boldsymbol{\mu}_i\cdot\mathbf{T}_{ij}\cdot\delta\boldsymbol{\mu}_j}\right\rangle=1+\frac{3}{2}\sum_{ij}\,\frac{\alpha_i\alpha_j}{r_{ij}^6}+\cdots. \tag{B11}$$

Back to expression (13), the two-body correction to the self-consistent field is

$$U^{\rm eff}(\{\mathbf{r}\})=U^{\rm SCF}(\{\mathbf{r}\})-\frac{3}{2}k_{\rm B}T\sum_{ij}\,\frac{\alpha_i\alpha_j}{r_{ij}^6}+\cdots. \tag{B12}$$

APPENDIX C: NUMERICAL INTEGRATORS

1. Nosé–Hoover thermostats

The Liouville operator corresponding to Eqs. (15) to (18) is

$$i\mathcal{L}=i\mathcal{L}_r+i\mathcal{L}_v+i\mathcal{L}_\eta+i\mathcal{L}_{\dot\eta}, \tag{C1}$$

where

$$i\mathcal{L}_r=\sum_i\,\left(\mathbf{v}_{\mathbf{R},i}\cdot\frac{\partial}{\partial\mathbf{R}_i}+\mathbf{v}_{\mathbf{d},i}\cdot\frac{\partial}{\partial\mathbf{d}_i}\right), \tag{C2}$$

$$i\mathcal{L}_v=\sum_i\,\left(\frac{\mathbf{F}_{\mathbf{R},i}}{m_i}\cdot\frac{\partial}{\partial\mathbf{v}_{\mathbf{R},i}}+\frac{\mathbf{F}_{\mathbf{d},i}}{m_i'}\cdot\frac{\partial}{\partial\mathbf{v}_{\mathbf{d},i}}\right), \tag{C3}$$

$$i\mathcal{L}_\eta=\dot\eta\frac{\partial}{\partial\eta}+\dot\eta_\star\frac{\partial}{\partial\eta_\star}-\sum_i\,\left(\eta\mathbf{v}_{\mathbf{R},i}\cdot\frac{\partial}{\partial\mathbf{v}_{\mathbf{R},i}}+\eta_\star\mathbf{v}_{\mathbf{d},i}\cdot\frac{\partial}{\partial\mathbf{v}_{\mathbf{d},i}}\right), \tag{C4}$$

$$i\mathcal{L}_{\dot\eta}=\frac{G}{Q}\frac{\partial}{\partial\dot\eta}+\frac{G_\star}{Q_\star}\frac{\partial}{\partial\dot\eta_\star}. \tag{C5}$$

Variables $\{\mathbf{v_R},\mathbf{v_d}\}$ are the conjugate velocities of $\{\mathbf{R},\mathbf{d}\}$.

The velocity-Verlet propagation [see Eq. (24)] is

$$e^{i\mathcal{L}_{\rm VV}\Delta t}\simeq e^{i\mathcal{L}_v\Delta t/2}\,e^{i\mathcal{L}_r\Delta t}\,e^{i\mathcal{L}_v\Delta t/2}. \tag{C6}$$

Applied to the left of a phase space vector $\mathbf{X}$, this sequence of three differential operators translates into a step of the usual velocity-Verlet algorithm.[90] Over a time interval $\tau=\Delta t/2n_{\rm c}$, the Nosé–Hoover propagation [see Eq. (24)] is

$$e^{i\mathcal{L}_{\rm NH}\tau}\simeq e^{i\mathcal{L}_{\dot\eta}\tau/2}\,e^{i\mathcal{L}_\eta\tau}\,e^{i\mathcal{L}_{\dot\eta}\tau/2}. \tag{C7}$$

Applied to $\mathbf{X}$, this sequence can also be translated into a simple algorithm.[71]

The overall propagation operator $e^{i\mathcal{L}\Delta t}$ can be written as pseudocode, to be read from right to left

$$\underbrace{e^{i\mathcal{L}_{\dot\eta}\tau/2}\,G\,e^{i\mathcal{L}_{\eta}\tau}\,e^{i\mathcal{L}_{\dot\eta}\tau/2}\,G}_{\text{repeat } n_c \text{ times}}\left(R_v\,e^{i\mathcal{L}_v\Delta t/2}\,F\,R_r\,e^{i\mathcal{L}_r\Delta t}\,e^{i\mathcal{L}_v\Delta t/2}\right)$$
$$\times\underbrace{e^{i\mathcal{L}_{\dot\eta}\tau/2}G\,e^{i\mathcal{L}_{\eta}\tau}\,e^{i\mathcal{L}_{\dot\eta}\tau/2}\,G}_{\text{repeat } n_c \text{ times}}. \tag{C8}$$

R_r and R_v stand for the SHAKE[70] and RATTLE[91] operations on the positions and on the velocities. F stands for the computation of the forces $\{\mathbf{F}\}$, after the update of the positions. G stands for the computation of "forces" G and $G_\star$, before every occurrence of $i\mathcal{L}_{\dot\eta}$.

2. Andersen–Hoover barostat

The Liouville operator for Eqs. (25) to (31) is

$$i\mathcal{L}=i\mathcal{L}_r^{\varepsilon}+i\mathcal{L}_v^{\varepsilon}+i\mathcal{L}_\eta+i\mathcal{L}_{\dot\eta}+i\mathcal{L}_\varepsilon+i\mathcal{L}_{\dot\varepsilon}, \tag{C9}$$

where $i\mathcal{L}_r^{\varepsilon}$ and $i\mathcal{L}_v^{\varepsilon}$ are extensions of $i\mathcal{L}_r$ and $i\mathcal{L}_v$

$$i\mathcal{L}_r^{\varepsilon}=\sum_i\left[(\mathbf{v}_{\mathbf{R},i}+\dot\varepsilon\mathbf{R}_i)\cdot\frac{\partial}{\partial\mathbf{R}_i}+(\mathbf{v}_{\mathbf{d},i}+\dot\varepsilon\mathbf{d}_i)\cdot\frac{\partial}{\partial\mathbf{d}_i}\right], \tag{C10}$$

$$i\mathcal{L}_v^{\varepsilon}=\sum_i\left[\left(\frac{\mathbf{F}_{\mathbf{R},i}}{m_i}-a\dot\varepsilon\mathbf{R}_i\right)\cdot\frac{\partial}{\partial\mathbf{v}_{\mathbf{R},i}}+\left(\frac{\mathbf{F}_{\mathbf{d},i}}{m_i'}-a\dot\varepsilon\mathbf{d}_i\right)\cdot\frac{\partial}{\partial\mathbf{v}_{\mathbf{d},i}}\right], \tag{C11}$$

and where

$$i\mathcal{L}_\varepsilon=\dot\varepsilon\frac{\partial}{\partial\varepsilon}, \tag{C12}$$

$$i\mathcal{L}_{\dot\varepsilon}=\frac{G_\varepsilon}{W}\frac{\partial}{\partial\dot\varepsilon}. \tag{C13}$$

G_ε corresponds to the right-hand side of Eq. (31).

We use a yet unpublished decomposition of the Andersen–Hoover barostat propagator proposed by Tuckerman,[73] where the barostat is treated along with the particles, but the thermostats are integrated separately, at the beginning and the end of each time step. The propagator can be written

$$e^{i\mathcal{L}\Delta t}\simeq(e^{i\mathcal{L}_{\mathrm{NH}}\Delta t/2n_c})^{n_c}e^{i\mathcal{L}_{\mathrm{vV}}^{\varepsilon}\Delta t}(e^{i\mathcal{L}_{\mathrm{NH}}\Delta t/2n_c})^{n_c}. \tag{C14}$$

The operator $e^{i\mathcal{L}_{\mathrm{NH}}\tau}$ is propagating the η and $\eta_\star$ thermostats as in Eq. (C7). The operator $e^{i\mathcal{L}_{\mathrm{vV}}^{\varepsilon}\Delta t}$ is a modified velocity-Verlet propagator that also propagates the barostat ε

$$e^{i\mathcal{L}_{\mathrm{vV}}^{\varepsilon}\Delta t}\simeq e^{i\mathcal{L}_{\dot\varepsilon}\Delta t/2}\,e^{i\mathcal{L}_v^{\varepsilon}\Delta t/2}\,e^{i\mathcal{L}_r^{\varepsilon}\Delta t}\,e^{i\mathcal{L}_\varepsilon\Delta t}\,e^{i\mathcal{L}_v^{\varepsilon}\Delta t/2}\,e^{i\mathcal{L}_{\dot\varepsilon}\Delta t/2}. \tag{C15}$$

Applied to $\mathbf{X}$, this sequence can be translated into a simple algorithm.

Constraints on the bond lengths are enforced with the SHAKE/Roll and RATTLE/Roll procedures of Martyna *et al.*[71] The $e^{i\mathcal{L}_{\mathrm{vV}}^{\varepsilon}\Delta t}$ propagator, applied from the left, is written in the following pseudocode:

$$\left(\underbrace{R_v^{\varepsilon}\,e^{i\mathcal{L}_{\dot\varepsilon}\Delta t/2}\,G_\varepsilon\,e^{i\mathcal{L}_v\Delta t/2}\,r\;s}_{\text{iterate until consistent}}\;F\;\underbrace{R_r^{\varepsilon}\,e^{i\mathcal{L}_r\Delta t}\,e^{i\mathcal{L}_\varepsilon\Delta t}\,e^{i\mathcal{L}_v\Delta t/2}\,e^{i\mathcal{L}_{\dot\varepsilon}\Delta t/2}\,G_\varepsilon\,r\;s}_{\text{iterate until consistent}}\right). \tag{C16}$$

F stands for the computation of the forces $\{\mathbf{F}\}$ and G_ε stands for the computation of "force" G_ε. R_r^{ε} and R_v^{ε} stand for the SHAKE/Roll and RATTLE/Roll operations, and the braces contain the operations to iterate to self-consistency. s and r stand for "store a copy of the phase vector $\mathbf{X}$" and "recall the copy of $\mathbf{X}$." The $e^{i\mathcal{L}_{\mathrm{NH}}\tau}$ propagator is as described in Appendix C 1.

[1] W. D. Cornell, P. Cieplak, C. I. Bayly, I. R. Gould, K. M. Merz, Jr., D. M. Ferguson, D. C. Spellmeyer, T. Fox, J. W. Caldwell, and P. A. Kollman, J. Am. Chem. Soc. **117**, 5179 (1995).
[2] A. D. MacKerell, Jr., D. Bashford, and M. Bellott *et al.*, J. Phys. Chem. B **102**, 3586 (1998).
[3] W. F. van Gunsteren, X. Daura, and A. E. Mark, in *Encyclopedia of Computational Chemistry*, edited by P. von Ragué Schleyer, N. L. Allinger, T. Clark, J. Gasteiger, P. A. Kollman, H. F. Schaefer III, and P. R. Schreiner (Wiley, New York, 1998), Vol. 2, pp. 1211–1216.
[4] W. L. Jorgensen and J. Tirado-Rives, J. Am. Chem. Soc. **110**, 1657 (1988).
[5] M. Karplus, Acc. Chem. Res. **35**, 321 (2002).
[6] W. L. Jorgensen, J. Chandrasekhar, J. D. Madura, R. W. Impey, and M. L. Klein, J. Chem. Phys. **79**, 926 (1983).
[7] H. J. C. Berendsen, J. P. M. Postma, W. F. van Gunsteren, and J. Hermans, in *Intermolecular Forces*, edited by B. Pullman (Reidel, Dordrecht, 1981), pp. 331–342.
[8] M. W. Mahoney and W. L. Jorgensen, J. Chem. Phys. **112**, 8910 (2000).
[9] J. Åqvist, J. Phys. Chem. **94**, 8021 (1990).
[10] D. Beglov and B. Roux, J. Chem. Phys. **100**, 9050 (1994).
[11] T. P. Lybrand and P. A. Kollman, J. Chem. Phys. **83**, 2923 (1985).
[12] S. J. Stuart and B. J. Berne, J. Phys. Chem. **100**, 11934 (1996).
[13] D. J. Tobias, P. Jungwirth, and M. Parrinello, J. Chem. Phys. **114**, 7036 (2001).
[14] L. X. Dang, J. Phys. Chem. B **106**, 10388 (2002).
[15] B. Roux and S. Bernèche, Biophys. J. **82**, 1681 (2002).
[16] T. A. Halgren and W. Damm, Curr. Opin. Struct. Biol. **11**, 236 (2001).
[17] S. W. Rick and S. J. Stuart, in *Reviews in Computational Chemistry*, edited by K. B. Lipkowitz and D. B. Boyd (Wiley-VCH, Hoboken, NJ, 2002), Vol. 18, pp. 89–146.
[18] D. van Belle, I. Couplet, M. Prevost, and S. J. Wodak, J. Mol. Biol. **198**, 721 (1987).
[19] S. W. Rick, S. J. Stuart, and B. J. Berne, J. Chem. Phys. **101**, 6141 (1994).
[20] L. Onsager, J. Am. Chem. Soc. **58**, 1486 (1936).
[21] J. G. Kirkwood, J. Chem. Phys. **7**, 911 (1939).
[22] E. L. Pollock and B. J. Alder, Phys. Rev. Lett. **39**, 299 (1977).
[23] P. Barnes, J. L. Finney, J. D. Nicholas, and J. E. Quinn, Nature (London) **282**, 459 (1979).
[24] P. Cieplak and P. Kollman, J. Chem. Phys. **92**, 6755 (1990).
[25] P. Cieplak and P. A. Kollman, J. Chem. Phys. **92**, 6761 (1990).
[26] B. T. Thole, Chem. Phys. **59**, 341 (1981).
[27] P. T. van Duijnen and M. Swart, J. Phys. Chem. A **102**, 2399 (1998).
[28] H. A. Stern, G. A. Kaminski, J. L. Banks, R. Zhou, B. J. Berne, and R. A. Friesner, J. Phys. Chem. B **103**, 4730 (1999).
[29] J. M. Goodfellow, Proc. Natl. Acad. Sci. U.S.A. **79**, 4977 (1982).

[30] Z.-H. Duan and R. Krasny, J. Chem. Phys. **113**, 3492 (2000).
[31] A. Toukmaji, C. Nagui, J. Board, and T. Darden, J. Chem. Phys. **113**, 10913 (2000).
[32] P. Cieplak, J. Caldwell, and P. Kollman, J. Comput. Chem. **22**, 1048 (2001).
[33] R. F. Nalewajski, J. Phys. Chem. **89**, 2831 (1985).
[34] W. J. Mortier, S. K. Ghosh, and S. Shankar, J. Am. Chem. Soc. **108**, 4315 (1986).
[35] A. K. Rappé and W. A. Goddard III, J. Phys. Chem. **95**, 3358 (1991).
[36] R. Chelli, P. Procacci, R. Righini, and S. Califano, J. Chem. Phys. **111**, 8569 (1999).
[37] J. L. Banks, G. A. Kaminski, R. Zhou, D. T. Mainz, B. J. Berne, and R. A. Friesner, J. Chem. Phys. **110**, 741 (1999).
[38] P. Drude, *The Theory of Optics* (Longmans, Green, New York, 1902), translation by C. Riborg Mann and Robert A. Millikan.
[39] F. London, Trans. Faraday Soc. **33**, 8 (1937).
[40] W. L. Bade, J. Chem. Phys. **27**, 1280 (1957).
[41] W. L. Bade and J. G. Kirkwood, J. Chem. Phys. **27**, 1284 (1957).
[42] A. T. Amos, Int. J. Quantum Chem. **60**, 67 (1996).
[43] F. Wang and K. D. Jordan, J. Chem. Phys. **116**, 6973 (2002).
[44] B. G. Dick and A. W. Overhauser, Phys. Rev. **112**, 90 (1958).
[45] J. E. Hanlon and A. W. Lawson, Phys. Rev. **113**, 472 (1959).
[46] G. Jacucci, I. R. McDonald, and K. Singer, Phys. Lett. A **50**, 141 (1974).
[47] M. J. L. Sangster and M. Dixon, Adv. Chem. Phys. **25**, 247 (1976).
[48] P. J. Mitchell and D. Fincham, J. Phys.: Condens. Matter **5**, 1031 (1993).
[49] P. J. D. Lindan and M. J. Gillan, J. Phys.: Condens. Matter **5**, 1019 (1993).
[50] J. S. Høye and G. Stell, J. Chem. Phys. **73**, 461 (1980).
[51] L. R. Pratt, Mol. Phys. **40**, 347 (1980).
[52] J. Cao and B. J. Berne, J. Chem. Phys. **99**, 2213 (1993).
[53] F. Lado, J. Chem. Phys. **106**, 4707 (1997).
[54] H. Saint-Martin, C. Medina-Llanos, and I. Ortega-Blake, J. Chem. Phys. **93**, 6448 (1990).
[55] N. H. de Leeuw and S. C. Parker, Phys. Rev. B **58**, 13901 (1998).
[56] H. Saint-Martin, J. Hernández-Cobos, M. I. Bernal-Uruchurtu, I. Ortega-Blake, and H. J. C. Berendsen, J. Chem. Phys. **113**, 10899 (2000).
[57] P. J. van Maaren and D. van der Spoel, J. Phys. Chem. B **105**, 2618 (2001).
[58] H. Yu, T. Hansson, and W. F. van Gunsteren, J. Chem. Phys. **118**, 221 (2003).
[59] S. J. Stuart and B. J. Berne, J. Phys. Chem. A **103**, 10300 (1999).
[60] M. Sprik and M. L. Klein, J. Chem. Phys. **89**, 7556 (1988).
[61] P. Ahlström, A. Wallqvist, S. Engström, and B. Jönsson, Mol. Phys. **68**, 563 (1989).
[62] C. J. F. Böttcher, *Theory of Electric Polarization. Volume 1: Dielectrics in Static Fields*, 2nd ed. (Elsevier Scientific, Amsterdam, 1973).
[63] G. Jacucci, I. R. McDonald, and A. Rahman, Phys. Rev. A **13**, 1581 (1976).
[64] M. W. Mahoney and W. L. Jorgensen, J. Chem. Phys. **114**, 9337 (2001).
[65] D. van Belle, M. Froeyen, G. Lippens, and S. J. Wodak, Mol. Phys. **77**, 239 (1992).
[66] D. V. Belle and S. J. Wodak, Comput. Phys. Commun. **91**, 253 (1995).
[67] R. W. Pastor, B. R. Brooks, and A. Szabo, Mol. Phys. **65**, 1409 (1988).
[68] W. G. Hoover, Phys. Rev. A **31**, 1695 (1985).
[69] M. Sprik, J. Phys. Chem. **95**, 2283 (1991).
[70] J. P. Ryckaert, G. Ciccotti, and H. J. C. Berendsen, J. Comput. Phys. **23**, 327 (1977).
[71] G. J. Martyna, M. E. Tuckerman, D. J. Tobias, and M. L. Klein, Mol. Phys. **87**, 1117 (1996).
[72] G. J. Martyna, D. J. Tobias, and M. L. Klein, J. Chem. Phys. **101**, 4177 (1994).
[73] M. E. Tuckerman, private communication (2001).
[74] S. C. Harvey, R. K.-Z. Tan, and T. E. Cheatham, III, J. Comput. Chem. **19**, 726 (1998).
[75] G. J. Martyna, M. L. Klein, and M. Tuckerman, J. Chem. Phys. **97**, 2635 (1992).
[76] M. E. Tuckerman, B. J. Berne, G. J. Martyna, and M. L. Klein, J. Chem. Phys. **99**, 2796 (1993).
[77] D. J. Tobias, G. J. Martyna, and M. L. Klein, J. Phys. Chem. **97**, 12959 (1993).
[78] S.-W. Chiu, M. Clark, S. Subramaniam, and E. Jakobsson, J. Comput. Chem. **21**, 121 (2000).
[79] B. R. Brooks, R. E. Bruccoleri, B. D. Olafson, D. J. States, S. Swaminathan, and M. Karplus, J. Comput. Chem. **4**, 187 (1983).
[80] T. Darden, D. York, and L. Pedersen, J. Chem. Phys. **98**, 10089 (1993).
[81] M. P. Allen and D. J. Tildesley, *Computer Simulation of Liquids* (Clarendon, Oxford, 1987).
[82] M. Neumann and O. Steinhauser, Chem. Phys. Lett. **106**, 563 (1984).
[83] B. L. Holian and A. F. Voter, Phys. Rev. E **52**, 2338 (1995).
[84] M. Sprik, J. Chem. Phys. **95**, 6762 (1991).
[85] J.-C. Soetens, M. T. C. M. Costa, and C. Millot, Mol. Phys. **94**, 577 (1998).
[86] A. Wallqvist and R. D. Mountain, in *Molecular Models of Water: Derivation and Description*, Vol. 13 of Reviews in Computational Chemistry edited by K. B. Lipkowitz and D. B. Boyd (Wiley-VCH, New York, 1999), Chap. 4, pp. 183–247.
[87] L. D. Site, A. Alavi, and R. M. Lynden-Bell, Mol. Phys. **96**, 1683 (1999).
[88] D. P. Fernandez, Y. Mulev, A. R. H. Goodwin, and J. M. H. L. Sengers, J. Phys. Chem. Ref. Data **24**, 33 (1995).
[89] A. A. Abrikosov, L. P. Gorkov, and I. E. Dzyaloshinski, in *Methods of Quantum Field Theory in Statistical Physics*, edited by R. A. Silverman (Dover, New York, 1975).
[90] W. Swope, H. Andersen, P. Berens, and K. Wilson, J. Chem. Phys. **76**, 637 (1982).
[91] H. C. Andersen, J. Comput. Phys. **52**, 24 (1983).
[92] *Water: A Comprehensive Treatise*, Vol. 1: The Physics and Physical Chemistry of Water, edited by F. Franks (Plenum, New York, 1972).
[93] J. Verhoeven and A. Dymanus, J. Chem. Phys. **52**, 3222 (1970).
[94] T. R. Dyke, K. M. Mack, and J. S. Muenter, J. Chem. Phys. **66**, 498 (1977).
[95] G. Jancsó and W. A. van Hook, Chem. Rev. **74**, 689 (1974).
[96] K. Krynicki, C. D. Green, and D. W. Sawyer, Discuss. Faraday Soc. **66**, 199 (1978).
[97] A. K. Soper, F. Bruni, and M. A. Ricci, J. Chem. Phys. **106**, 247 (1997).